

Journal of Turbulence



ISSN: 1468-5248 (Online) Journal homepage: www.tandfonline.com/journals/tjot20

Cross-validation of numerical and experimental data in turbulent pipe flow with new scaling correlations

El-Sayed Zanoun, Christian Bauer, Claus Wagner, Franz Durst, Christoph Egbers, Gabriele Bellani & Alessandro Talamelli

To cite this article: El-Sayed Zanoun, Christian Bauer, Claus Wagner, Franz Durst, Christoph Egbers, Gabriele Bellani & Alessandro Talamelli (16 Oct 2025): Cross-validation of numerical and experimental data in turbulent pipe flow with new scaling correlations, Journal of Turbulence, DOI: 10.1080/14685248.2025.2560314

To link to this article: https://doi.org/10.1080/14685248.2025.2560314

9	© 2025 The Author(s). Published by Informa UK Limited, trading as Taylor & Francis Group.
	Published online: 16 Oct 2025.
	Submit your article to this journal $oldsymbol{oldsymbol{\mathcal{G}}}$
hil	Article views: 43
Q ^L	View related articles 🗗
CrossMark	View Crossmark data 🗗







Cross-validation of numerical and experimental data in turbulent pipe flow with new scaling correlations

El-Sayed Zanoun [©]^a, Christian Bauer^b, Claus Wagner^{b,c}, Franz Durst^d, Christoph Egbers^a, Gabriele Bellanie and Alessandro Talamellie

^aDepartment of Aerodynamics and Fluid Mechanics, BTU Cottbus-Senftenberg, Cottbus, Germany; ^bInstitute of Aerodynamics and Flow Technology, German Aerospace Center (DLR), Göttingen, Germany; ^cInstitute of Thermodynamics and Fluid Mechanics, Technische Universität Ilmenau, Ilmenau, Germany; ^dLSTM-Erlangen, FAU Erlangen-Nuremberg, Erlangen, Germany; ^eDepartment of Industrial Engineering, University of Bologna, Forli, Italy

ABSTRACT

The dependence of turbulence statistics and wall friction on Reynolds number in fully developed turbulent pipe flow remains a fundamental subject in fluid mechanics. This paper cross-validates experimental and numerical results, focusing on the scaling of turbulence statistics at the pipe centerline and across the inner-outer flow region. Pipe flow experiments were reviewed for friction Reynolds numbers $810 \le \text{Re}_{\tau} \le 55 \times 10^3$, where $\text{Re}_{\tau} = u_{\tau}R/\nu$, u_{τ} is the wall friction velocity, R the pipe radius, and ν the kinematic viscosity. Complementary DNS data for $180 \le \text{Re}_{\tau} \le 2880$ provide detailed insight into near-wall turbulence. A novel friction correlation, $\text{Re}_{\tau} = 0.048 \, \text{Re}_{c}^{0.923}$ is introduced, predicting pipewall friction across a wide range of Re_c with accuracy better than $\pm 2.06\%$, where Re_c is the Reynolds number based on the centerline streamwise mean velocity component \overline{U}_{zc} . This correlation enables reliable friction estimates from centerline single-point measurements or DNS data without requiring near-wall or streamwise pressure-gradient information and is validated by consistent agreement with both experiments and DNS. The monotonic decrease in centerline turbulence intensity $\langle u_z'^2 \rangle^{1/2}/\overline{U}_{zc}$ with increasing Re_c is explained using the streamwise mean momentum equation. Finally, azimuthal spatial filtering of DNS data highlights the limitations of hot-wire resolution near the wall. For Re_{τ} \geq 2880, higher-order experimental statistics agree well with DNS for $y^+ \ge 30$ and into the logarithmic region, with both datasets equally well described by logarithmic or power-law correlations, while near-wall discrepancies remain due to resolution limits.

ARTICLE HISTORY

Received 26 November 2024 Accepted 3 September 2025

KEYWORDS

Pipe flow; turbulence statistics; DNS; experiments

1. Introduction

Experimental and numerical studies of wall-bounded turbulent shear flows, including boundary layer, pipe and channel flows, have progressed over several decades [1–23], providing valuable insights into the statistics of wall turbulence. Gad-el Hak and Bandyopadhyay [4] gave a detailed review of turbulence statistics, highlighting important issues related to the effects of Reynolds number on turbulent pipe flow statistics and scaling in both the logarithmic overlap region and near the wall. In the immediate vicinity of the wall, researchers often face challenges due to the Reynolds number effect and limited spatial resolution, making it difficult to obtain reliable experimental and numerical turbulence data, for example, the components of the Reynolds stress tensor and higher-order statistics, see [5,6,24-26]. Discrepancies in the literature regarding the Reynolds number dependence of near-wall turbulence statistics are claimed to be due to variations in the spatial resolution and the accuracy of both experimental and numerical methods. Recent experiments on near-wall turbulence in pipe flows, such as those of Hultmark et al. [11], have shown that the near-wall peak of the streamwise velocity fluctuations $\langle u_z^2 \rangle^+$ remains invariant in both location and magnitude with respect to Reynolds number up to Re_b = 145,000, where Re_b = $\overline{U}_{zb}D/\nu$ is defined based on the bulk velocity \overline{U}_{zb} , the pipe diameter D, and the kinematic viscosity ν . This finding is consistent with a similar conclusion made by Mochizuki and Nieuwstadt [8] regarding the magnitude of the $\langle u_z^2 \rangle^+$ -peak value; however, they found its location to be slightly dependent on the Reynolds number. This finding, however, contrasts with the results of [2,9,13,17,22] as well as with the present pipe flow experiments and simulations, which show a significant dependence of the magnitude of the $\langle u_z'^2 \rangle^+$ -peak value on the Reynolds number. Despite these differences, the near-wall peak position of $\langle u_z'^2 \rangle^+$ remains fixed at the same wall-normal position identified by many authors, e.g. [4,9,11,13,15,17,22]. The spatial resolution of the measurement probe and/or the grid spacing play a crucial role in accurately capturing the turbulence statistics, and their effects may overlap with the Reynolds number effect. Furthermore, the lack of accurate higher-order moments, i.e. skewness and flatness, remains a persistent problem, especially from an experimental perspective, and this problem becomes more pronounced at higher Reynolds numbers, due to the extremely thin viscous sublayer and the near-wall limited spatial resolution. Therefore, the present authors incorporate turbulence statistical data from direct numerical simulations [18,27] to complement near-wall experimental studies.

Another area of focus in the fluid mechanics community is the scaling of turbulence statistics, both in the near-wall region and the pipe core. In the wall layer, the friction velocity, $u_{\tau} = \sqrt{\tau_w/\rho}$, and the viscous length scale, $\ell_c = v/u_\tau$, are commonly used as the traditional turbulence scales, where τ_w is the wall shear stress. Accurate scaling in the core region is essential for characterising different turbulent structures [28,29]. In pipe flow, the centreline mean velocity \overline{U}_{zc} and the pipe radius R are typically adopted as the velocity and length scales for core turbulence scaling [9,12,13]. The work of Morrison et al. [9] and Marusic et al. [12] suggested that a unified scaling approach considering both the inner and outer/core regions would be appropriate to accurately describe the centreline turbulence behaviour under varying flow conditions. Their refined approach via the so-called Kármán/friction number, $Re_{\tau} = R/\ell_c$, helps bridge the gap between near-wall and core flow characteristics. Its definition connects two relevant length scales - viscous (ℓ_c) to integral/large (R) scales – as an appropriate similarity parameter. In the present study, therefore, the friction Reynolds number Re_{τ} is adopted as an appropriate similarity parameter. Careful experiments were conducted using pipe facilities at LSTM-Erlangen (1492 \leq Re_{τ} \leq 8597) [30,31], BTU Cottbus-Senftenberg (CoLaPipe) (3441 \leq Re_{τ} \leq 17,608) [32] and the University of Bologna (CICLoPE) (6566 \leq Re_{τ} \leq 38,203) [33]. These pipe experiments were designed to provide insight into pipe flow statistics and scaling. In addition, the pipe-flow experimental statistics were supplemented with available DNS data from Bauer et al. [18] and Bauer [27]. They [18,27] investigated the convergence and scaling of high order statistics in turbulent pipe flows for friction Reynolds numbers in the range $180 \le \text{Re}_{\tau} \le 2880$.

The wall friction velocity, as discussed above, is a key scaling parameter in wall-bounded shear flows. Various friction relations have been extensively used and thoroughly discussed by Zanoun et al. [21]. One of the most established models is the Prandtl-von Kármán logarithmic law, which has served as a reliable framework for predicting the wall skin friction in turbulent shear flows. However, concerns have arisen about its accuracy, particularly at high Reynolds numbers [21,34], with experimental data showing deviations from predicted values. These discrepancies are often attributed to the limitations of the flow similarity assumptions inherent in the Prandtl-von Kármán model, which in particular fails to account for variations in the near-wall flow behaviour with the Reynolds number. Recent studies, see e.g. [21,34,35], have focussed on refining friction relations to address these limitations over a wider range of Reynolds numbers. However, the present study adopts a robust approach by determining pipe wall friction based on some integral flow parameters, thus reducing the influence of near-wall effects. In this context, the present study aims at mutual validation of measurements and DNS data, focussing on three key concerns related to pipe flow: (1) how turbulence statistics at the pipe centreline scale with the Reynolds number, (2) the measurement of the wall friction velocity as a critical scaling parameter [21], (3) the effect of the Reynolds number on the scaling of the mean velocity and higher order statistics [1-23]. To address these concerns, the frequency response and spatial resolution of measurement techniques such as hot-wire probes as well as their calibrations must be carefully considered. Uncertainties in probe positioning relative to the wall surface [36], as well as the locality of the wall friction velocity u_{τ} [21], are also critical factors. Through the analysis of complementary experimental (810 \leq Re_{τ} \leq 55 \times 10³) and numerical (180 \leq Re_{τ} \leq 2880) data, this work explores the effects of the Reynolds number on turbulence statistics, particularly at the pipe centreline and in the inner-outer overlap, while also investigating the scaling laws of higher-order statistical moments. The synergy between experiments and DNS is particularly valuable, as it covers a wide range of Reynolds numbers and provides insights into pipe wall friction and turbulence behaviour across the entire flow field, an analysis that cannot be achieved by experiments or simulations alone. This approach is essential for a better understanding



of flow characteristics in various engineering applications, such as fluid transport, friction, and process design.

To outline, the paper is organised into 4 sections. Following the introduction, Section 2 briefly describes the experimental facilities, measurement techniques, and DNS data sets used. Section 3 discusses the effects of Reynolds number on wall friction, the scaling of the mean flow, and the higher-order statistics of fully developed turbulent pipe flow. Finally, Section 3 presents conclusions and final remarks, along with suggestions for further work.

2. Experimental and numerical facilities

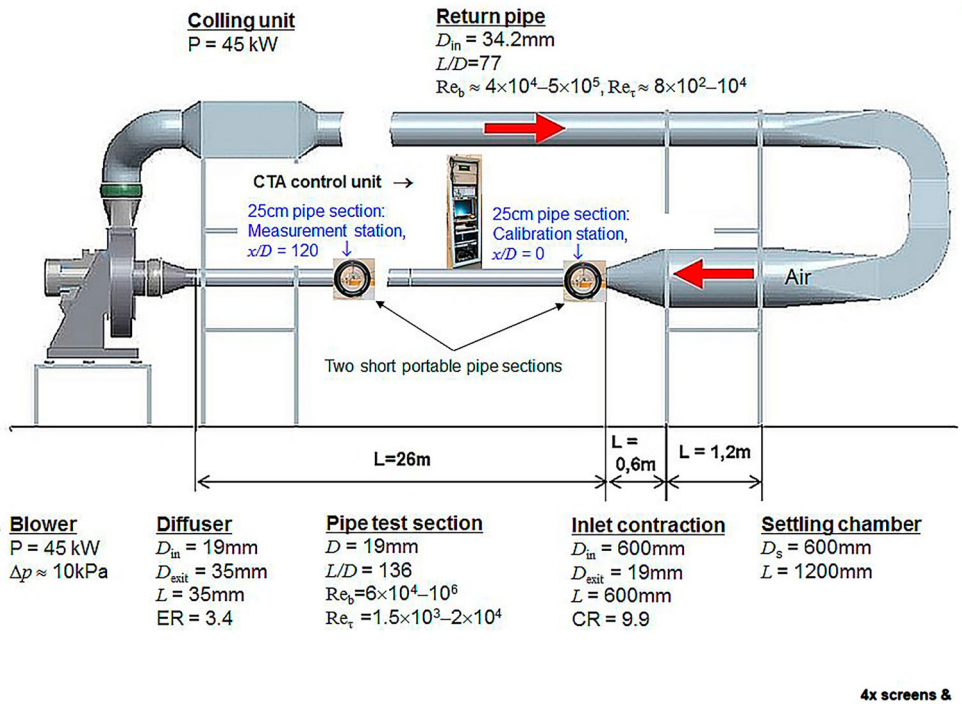
As summarised above, at high Reynolds numbers, experiments may face limitations if the measuring probe is not small enough and sampling frequency is not sufficiently high. When such constraints arise, corrections must be applied to obtain reliable near-wall statistics. Although decreasing grid spacing and time scales pose challenges for Direct Numerical Simulations (DNS) at high Reynolds numbers, DNS can still effectively resolve near-wall turbulence if sufficiently high spatial and temporal resolutions are used. Therefore, the combination of numerical and experimental techniques, supported by analytical methods, enables the investigation of turbulent shear flows across a wide range of Reynolds numbers. Present measurements have been performed in the large pipe facility CoLaPipe [32], located at the Department of Aerodynamics and Fluid Mechanics (LAS), Brandenburg University of Technology (BTU C-S), for friction Reynolds number Re_τ in the range $3441 \le \text{Re}_{\tau} \le 17,608$. The CoLaPipe, Figure 1 (top), is a closed return wind tunnel facility. It provides air with \approx 80 m/s maximum velocity, having a turbulence level less than 0.5% at the pipe inlet section [23]. It has two pipe sections, both made of high-precision smooth acrylic glass, having inner pipe diameters of 190 \pm 0.23 mm and 342 \pm 0.35 mm, with 136, and 77 length-to-diameter ratio (L/D) for suction and return sections, respectively. In addition, the CICLoPE pipe facility [33], Figure 1 (bottom), has been used to extend the CoLaPipe friction Reynolds number working range. The CICLoPE is also a closed return facility, located at the Interdepartmental Centre for Industrial Aerospace Research-CIRI Aerospace, University of Bologna, Italy, for a wider range of friction Reynolds number 6566 \leq Re_{τ} \leq 38,203.

The CICLoPE has a pipe section of 900 \pm 0.2 mm inner diameter, and 111.5 m total length, i.e. L/D=124, providing air with 60 m/s maximum velocity. Note that both facilities are equipped with water coolers to stabilise the air temperature inside the test sections. In both facilities, the ambient pressure and the temperature inside the test chamber were measured using an MKS Baratron 120A absolute pressure transducer and a PT 100 thermistor, respectively.

Hot-wire setup

In the CoLaPipe facility, streamwise velocity measurements have been conducted using both the Dantec Multichannel Constant Temperature Anemometer (CTA) and the Dantec Streamline hot-wire anemometer with commercial Dantec boundary layer probe, Model 55P53, see Table 1. In the CICLoPE facility, Dantec Streamline 90N10 CTA and Dantec 55P11 commercial probes were used in addition to custom–made Platinum single–wire probe [33], see Table 1. The selection of sampling frequency and time is crucial to ensure accurate measurements when using hot-wire, see [37,38]. According to the Nyquist-Shannon Sampling Theorem, the sampling frequency was typically chosen. Bruun [38] suggests, for instance, sampling frequencies in the range of 10 kHz to 100 kHz for turbulence measurements in turbulent flow. This range allows to capture high-frequency turbulent fluctuations without aliasing. Thus, in alignment with [37,38] and based on the viscous length and time scales associated with the Reynolds numbers summarised in Table 1, the sampling frequencies were set to 30 kHz & 60 kHz with low–pass filters at $f_{LP} = 15$ kHz & 30 kHz, for CoLaPipe and CICLOPE, respectively. Samples were acquired over 60–160 seconds, depending on the Reynolds number, at each measuring point, ensuring reliable time-averaged turbulence statistics.

Table 1 shows the principal parameters governing the flow conditions as well as details concerning the spatial and temporal resolution of the data for various pipe facilities. The spatial resolution of hot-wire is expressed non-dimensionally as $\ell_{hw}^+ = \ell_{hw} u_\tau / v$. Hot-wire had an aspect ratio $\ell_{hw}/d_{hw} \ge 250$ sufficiently large to suggest a negligible influence of the prongs on the velocity measurements. A fourth-degree polynomial was used for hot-wire calibration with an accuracy better than $\pm 1\%$. To ensure consistency, the calibration



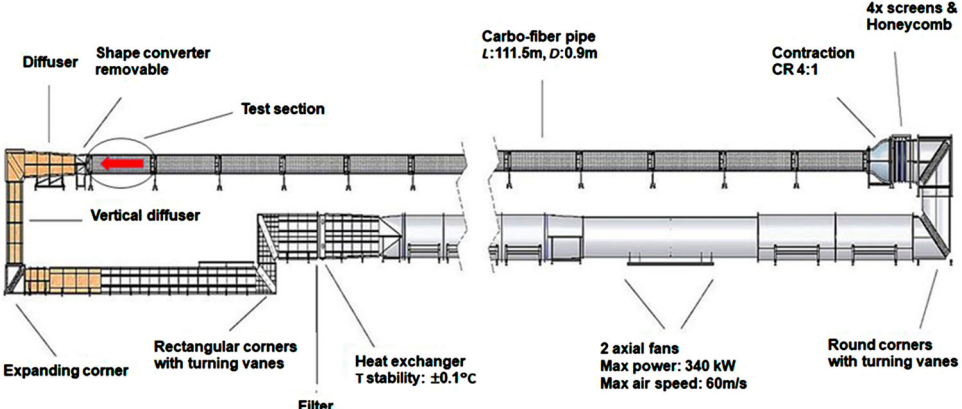


Figure 1. Pipe experimental facilities: (top) CoLaPipe at LAS, BTU C-S [32], (bottom) CICLoPE at CIRI, University of Bologna [33].

curve was rechecked after each set of measurements to cover the full velocity range in the near-wall region. The air stream temperature in all pipe facilities was kept constant within $\pm 0.2^{\circ}$ C during both calibration and measurements to ensure accurate velocity results. Once the calibration curve and least squares fitting equation were established, flow field measurements were conducted.

Pressure scanner and mean pressure gradient

It is known that the wall shear stress is directly related to the streamwise mean pressure gradient measured along the pipe test section. Therefore, the mean pressure gradient was measured, where the flow was confirmed to be fully developed in all pipe facilities, and these measurements were used to determine the wall friction velocity u_{τ} [21]. In The CoLaPipe facility, a 16-channel pressure scanner with a 7 kPa piezo-electric transducer was used for pressure measurements along the pipe test section. The transducer has frequency response up to 500 Hz/channel with measurement resolution of $\pm 0.003\%$ full scale. It was calibrated to compensate for offset, sensitivity, nonlinearity, and thermal effects. The wall pressure along the pipe test section was measured using wall pinholes and static pressure taps. For accurate mean pressure measurements, the ratio of the pinhole diameter d to the viscous length scale ℓ_c , i.e. d/ℓ_c , is indeed a critical factor, as discussed in [39]. A small d/ℓ_c ratio makes the flow through the hole highly sensitive to local pressure gradients and

Table 1. Summary of main experimental parameters from LSTM-Erlangen pipe, CoLaPipe and CICLoPE [33] facilities: Re_c =centreline Reynolds number, Re_τ =friction Reynolds number, $\ell_{\rm hw}$ =hot-wire length, $d_{\rm hw}$ =hot-wire diameter, $\ell_{\rm hw}^+=\ell_{\rm hw}u_{\tau}/\nu$ spanwise hot-wire length in wall units, $\ell_c = v/u_\tau$ viscous length scale, T_{hw} =sampling time.

Re _c	Re _τ [—]	u_{τ} [m/s]	ℓ _{hw} [μm]	d _{hw} [μm]	ℓ_{hw}/d_{hw} [–]	ℓ ⁺ [−]	<i>ℓ_c</i> [μm]	<i>T_{hw}</i> [s]
LSTM-Erlan	gen							
D = 112 mn	-							
70,271	1492	0.203	1.25	5	250	17	38	60
80,063	1620	0.442	1.25	5	250	36	35	60
94,543	1944	0.530	1.25	5	250	43	29	60
135,928	2668	0.725	1.25	5	250	60	21	60
160,248	3136	0.870	1.25	5	250	70	18	60
198,647	3838	1.075	1.25	5	250	86	15	60
231,504	4362	1.235	1.25	5	250	97	13	60
LSTM-Erlan	gen							
D = 148 mn	n [30,31]							
142,517	2687	0.547	1.25	5	250	45.5	27.3	60
198,918	3685	0.750	1.25	5	250	62	20.1	60
255,748	4722	0.990	1.25	5	250	80	15.7	60
306,957	5612	1.169	1.25	5	250	95	13.2	60
336,490	6134	1.228	1.25	5	250	104	12.1	60
365,363	6663	1.360	1.25	5	250	112	11.1	60
394,908	7153	1.433	1.25	5	250	121	10.1	60
420,486	7539	1.538	1.25	5	250	127	9.8	60
460,649	8182	1.627	1.25	5	250	138	9.0	60
486,242	8597	1.718	1.25	5	250	145	8.6	60
CoLaPipe-C								
D = 190 mn				_				
181,186	3441	0.5406	1.25	5	250	45	28	120
216,827	4130	0.6629	1.25	5	250	54	23	120
261,977	4845	0.7613	1.25	5	250	64	20	120
299,285	5462	0.8651	1.25	5	250	72	17.4	120
376,737	6752	1.0788	1.25	5	250	89	14.1	120
471,098	8287	1.3301	1.25	5	250	109	12	120
597,975	10,321	1.6691	1.25	5	250	136	9.2	120
675,904	11,527	1.8503	1.25	5	250	151	8.2	120
748,632	12,764	2.0911	1.25	5	250	168	7.5	120
834,484	13,989	2.2454	1.25	5	250	184	6.8	120
917,716	15,407	2.525	1.25	5	250	203	6.2	120
1,068,237	17,608	2.825	1.25	5	250	229	5.5	120
CICLoPE-Bo	-							
D = 900 mn		0.2670	0.7	2.5	200	17	42	160
634,364	10,847	0.3678	0.7	2.5	280	17	42	160
899,565	15,017	0.5092	0.7	2.5	280	23	30 24	160
1,162,960	19,085	0.6471	1.1	5 5	220	47 57	24	120
1,433,162	23,203	0.7867	1.1		220	57	20	120
1,709,693	27,373	0.9281	0.7	2.5	280	43	17 15	80
1,981,788	31,441	1.0660	0.7	2.5	280	49 55	15 12	80
2,255,750	35,508	1.2039	0.7	2.5	280	55	13	80
2,438,220	38,203	1.2953	0.7	2.5	280	60	12	80

viscous effects, resulting in a more complex relationship between the measured pressure and the overall pressure drop in the pipe. Conversely, a too large pinhole can reduce sensitivity to local flow variations, potentially sacrificing resolution for finer variations. Therefore, in turbulent flows, a sufficiently large pinhole provides a more stable measurement, as it minimises the effect of localised flow disturbances. A pinhole diameter d of 500 μ m was chosen, large enough compared to viscous length scale, see Table 1, with a depth ℓ of 2 mm, giving an aspect ratio of $\ell/d = 4$ [39]. The inner surface of the pipe was smoothed around the pressure pinholes to ensure accurate measurements. Pressure readings were taken simultaneously at 16 different locations, 8 meters downstream from the pipe inlet. The measurement points were spaced 0.5 meters apart in the streamwise direction, where fully-developed flow conditions were confirmed.

Similarly, in the CICLoPE pipe facility, the static pressure along the pipe was measured using 1000 µm pressure pinholes [33]. The pressure pinholes/taps were located in a 5 m long pipe test section, all 1m apart from each other. The first pressure location has 4 pinholes/taps azimuthally spaced, while the rest had a single pressure pinhole/tap at each location. Static pressure along the pipe was acquired with a 32-channel digital

Table 2. Summary of the turbulent pipe flow simulation cases [18,27]: $\text{Re}_{\tau} = u_{\tau}R/\nu$ and $Re_b = \overline{U}_{zb}D/v$ are the friction and bulk Reynolds numbers, where u_{τ} is the friction and \overline{U}_{zb} is the bulk velocity (D = 2R).

Case	P180	P360	P720	<i>P</i> 1500	P2880
Re_{τ}	180	360	720	1500	2880
Re _b	5258	11,664	25,992	60,075	123,260
L/R	42	42	42	42	42
N_z	1536	3072	4608	8192	12,288
N_{φ}	256	512	1024	2048	4096
Nr	84	160	222	408	646
Δz^+	4.9	4.9	6.6	7.7	9.8
$\operatorname{Re}_{\tau} \Delta \varphi$	4.4	4.4	4.4	4.6	4.4
Δr_{min}^+	0.31	0.39	0.49	0.49	0.32
$\Delta r_{min}^+ \ \Delta r_{max}^+$	4.4	4.4	4.6	6.8	4.4
$\Delta t u_{\tau}/D$	2×10^{-5}	1.5×10^{-5}	7×10^{-6}	3.2×10^{-6}	1.6×10^{-6}
ΔT_b	29,396	2838	788	310	31
ΔT^{+}	361,880	63,074	31,450	23,230	4183

Notes: N_z , N_{φ} , and N_r are the number of grid points with respect to the axial, azimuthal, and radial direction, respectively. Δz^+ , streamwise grid spacing; $Re_{\tau} \Delta \varphi$ azimuthal grid spacing at the wall; Δr_{min}^+ and Δr_{max}^+ , minimal and maximal radial grid spacing, respectively, all grid spacings normalised by wall units. Δt , simulation time step; ΔT , averaging interval for statistics; $\Delta T_b = \Delta T \overline{U}_{zb}/R$, in bulk time units; $\Delta T^+ =$ $\Delta T u_{\tau}^2 / v$, in viscous time units; Pipe length for all cases: L/R = 42.

pressure scanner Initium with a 2500 Pa range. Dynamic pressure was measured with MKS Baratron 120AD differential pressure transducer, with a range of 1333 Pa and an acquisition frequency of 10 Hz. In addition, the local mean centreline velocity was measured with a fixed L-shaped Prandtl tube.

DNS data sets

The experimental data at the lower end of the accessible Reynolds number range presented in Table 1 are compared to the DNS data sets of Bauer et al. [18] and Bauer [27] presented in Table 2. The DNS calculations were performed using a well-validated fourth-order finite-volume method suitable for solving the incompressible Navier-Stokes equations on a staggered grid for the domain of a smooth-walled pipe. As indicated in Table 2, the grid spacing in wall units was set to values of $\Delta z^+ \leq 9.8$ in the streamwise direction, Re₇ $\Delta \varphi \leq 4.6$ in the azimuthal direction at the wall, Δr^+ min ≤ 0.49 at the wall, and Δr^+ max ≤ 7.0 at the centreline, respectively. The grid refinement towards the wall is based on a hyperbolic tangent function. The one-point statistical quantities presented in this paper were computed using on-the-fly averaging in the axial and azimuthal directions as well as in time. For more details on the numerical methodology, the reader is referred to Bauer et al. [18].

3. Results and discussion

Streamwise mean momentum equation

For fully developed turbulent pipe flow, the relationship between the streamwise mean velocity, the pressure gradient, and the Reynolds stresses is governed by the well-known streamwise momentum equation:

$$\frac{\partial}{\partial z} \left[-\rho \overline{u_z' u_z'} + \rho \overline{U}_z^2 \right] + \frac{\partial}{\partial r} \left[\mu \frac{\partial \overline{U}_z}{\partial r} + (-\rho \overline{u_z' u_r'}) \right] = \frac{\partial \overline{p}}{\partial z}. \tag{1}$$

At the pipe centreline, where wall shear effects vanish as $\partial \overline{U}_z/\partial r \to 0$, the streamwise momentum equation reduces primarily to a balance between the mean pressure gradient and the streamwise component of Reynolds stress. This simplified relationship will be central to the analysis of streamwise turbulence statistics, particularly at the pipe centreline.

Friction factor

For fully developed turbulent pipe flow, all derivatives with respect to the streamwise direction, z, are zero, except for the mean pressure gradient $\partial \bar{p}/\partial z$, which is necessary to drive the flow against the pipe wall friction.

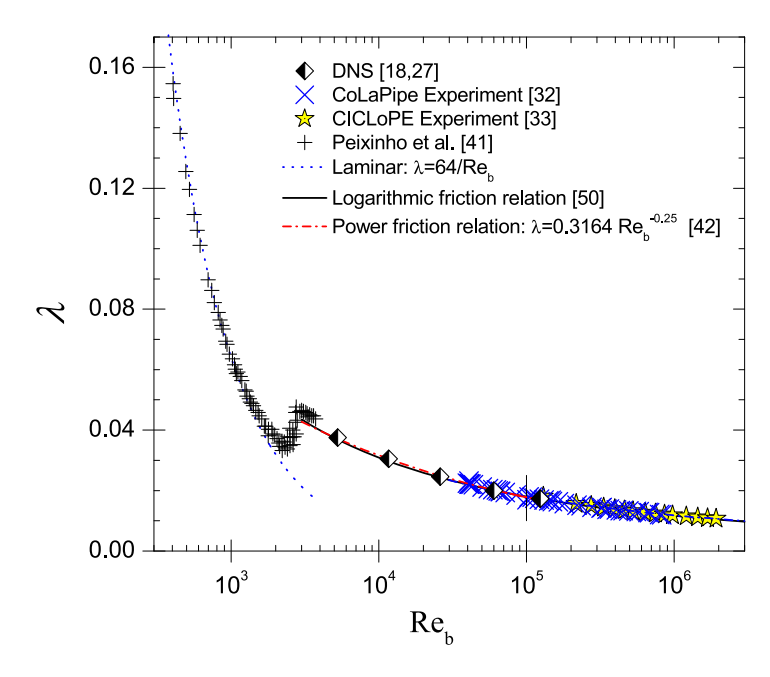


Figure 2. The pipe friction factor λ versus the bulk Reynolds number Re_b from various pipe facilities in fully-developed laminar and turbulent flow regimes $4 \times 10^2 \le \text{Re}_b \le 2 \times 10^6$.

Based on the boundary conditions on the pipe wall and centreline [40], the streamwise mean momentum Equation (1) can be written as:

$$\mu \frac{\partial \overline{U}_z}{\partial r} = -\frac{R}{2} \frac{\partial \overline{p}}{\partial z} \to \tau_w = -\frac{R}{2} \frac{\partial \overline{p}}{\partial z},\tag{2}$$

which indicates an exact balance between the wall shear stress τ_w and the mean pressure gradient $\partial \overline{p}/\partial z$ that drives the flow. Noting that $\tau_w = \mu \partial \overline{U}_z/\partial r$, and that $u_\tau = \sqrt{\tau_w/\rho}$ the wall friction velocity is regarded an appropriate scaling velocity for the entire shear layer, including the core region of the pipe [4].

Based on the wall friction velocity u_{τ} and the fluid bulk velocity \overline{U}_{zb} , the pipe friction factor λ is defined as $\lambda = 8(u_{\tau}/\overline{U}_{zb})^2$. The evolution of λ as a function of the Reynolds number based on bulk Re_b is presented in Figure 2.

In the laminar flow regime $Re_b \leq 2000$, good agreement is observed between the experiments carried out by Peixinho et al. [41] and the generalised Hagen-Poiseuille friction law $\lambda = 64/Re_b$ [42]. For fully developed turbulent pipe flow, both the pipe facilities at BTU C-S [32] and Bologna University [33] have been used to measure pipe wall friction for a wide range of Reynolds numbers [21]. Precise measurements of \overline{U}_{zb} and $\partial \overline{p}/\partial z$ along both pipe test sections were carried out, resulting in accurate pipe wall friction data presented in Figure 2, independently of the mean velocity profile. Figure 2 also depicts various sets of pipe friction data, including DNS data [18,27] in comparison with the friction relations discussed in [21]. The figure illustrates for $Re_b \leq 10^5$ an excellent agreement of the ColaPipe, CICLoPipe, and DNS data with the Blasius friction relation [42] $\lambda = 0.3164 \, Re_b^{-0.25}$. For $Re_b \geq 10^5$, the data showed a high degree of correlation with the various logarithmic friction relations discussed in [21].

Local mean flow properties

At the pipe centreline, the local streamwise mean velocity \overline{U}_{zc} and its velocity fluctuation u'_{zc} was measured and simulated at different Reynolds numbers $\text{Re}_c = \overline{U}_{zc}D/\nu$ based on the centreline velocity \overline{U}_{zc} at a streamwise location where the pipe flow was fully developed [18,27,30]. The intensity of the streamwise turbulence at the centreline, $\langle u'_{zc}^2 \rangle^{1/2}/\overline{U}_{zc}$, obtained from the DNS [18,27] and various experiments [1,3,30,31,43] is compared with recent results from the CoLaPipe [32] and CICLoPE [33] in Figure 3. The figure illustrates a monotonic decrease in $\langle u'_{zc}^2 \rangle^{1/2}/\overline{U}_{zc}$ as the Reynolds number Re_c increases. This monotonic decrease in the

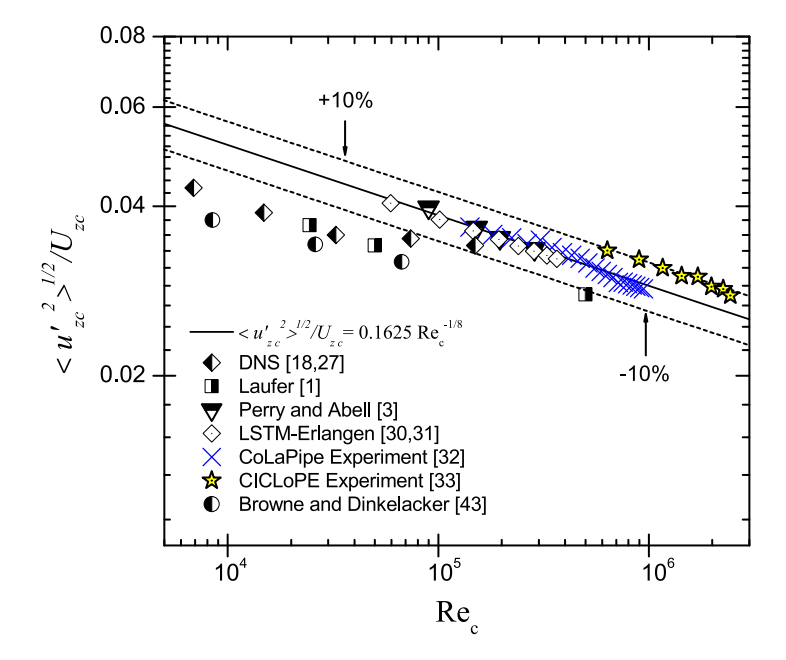


Figure 3. The centreline turbulence level $\sqrt{u_{zc}^{'2}}/\overline{U}_{zc}$ for fully-developed turbulent pipe flow from different pipe experiments [1,3,30–33,43] for $5 \times 10^3 \le \text{Re}_c \le 2.44 \times 10^6$ and simulations [18,27] for $6886 \le \text{Re}_c \le 149,261$.

centreline streamwise velocity fluctuations with increasing Reynolds number can be explained by examining the momentum equation of the streamwise velocity component, i.e. Equation (1), where $\mu \partial \overline{U}_z/\partial r$ is the viscous shear stress or the momentum transport due to the mean flow, $-\rho \overline{u_z'} \overline{u_r'}$ is the turbulent momentum transport due to the fluctuating velocities, and $\partial \overline{p}/\partial z$ is the gradient of the mean pressure in the streamwise direction.

On the one hand, in Equation (1), the velocity fluctuations – either u_z' or u_r' – are proportional to the square root of the mean pressure gradient in the streamwise direction. On the other hand, in Equation (2), the gradient of the mean velocity field $\partial \overline{U}_z/\partial r$ is directly proportional to the gradient of the mean pressure $\partial \overline{p}/\partial z$. Thus, as the Reynolds number increases, the growth rate of the local mean velocity at the centreline \overline{U}_{zc} surpasses that of the centreline velocity fluctuation, u_{zc}' . This results in a monotonic decrease in the centreline turbulence level $\langle u_{zc}'^2 \rangle^{1/2}/\overline{U}_{zc}$ as a function of the Reynolds number Re_c as shown in Figure 3. The figure shows satisfactory agreement between the experimental results from CoLaPipe for 181,186 \leq Re_c \leq 1,068,237 versus data extracted from the literature [3,30,43] for the fully-developed turbulent pipe flow. Using least-squares curve fitting, the normalised streamwise centreline velocity fluctuation $\langle u_{zc}'^2 \rangle^{1/2}/\overline{U}_{zc}$ from CoLaPipe with data, combined with data extracted from [3,30,31] for Re_c \geq 10⁵ yields the following relation:

$$\frac{\langle u'_{zc}^2 \rangle^{1/2}}{\overline{U}_{zc}} = 0.1625 \,\text{Re}_c^{(-1/8)} \tag{3}$$

Equation (3) reproduces $\langle u_{zc}^{\prime}^2 \rangle^{1/2} / \overline{U}_{zc}$ with $\pm 1.717\%$ uncertainty for $\text{Re}_c \geq 10^5$. By contrast, the experimental data sets [1,33,43] show less agreement with Equation (3) which may be attributed to low Reynolds number effects and/or to the accuracy of measuring the local turbulence statistics at the centreline. However, the experimental data at low Reynolds numbers from [1,43] are in close agreement with the DNS data [18,27].

Furthermore, the mean velocity at the centreline \overline{U}_{zc} is normalised with the bulk velocity \overline{U}_{zb} for various Reynolds numbers and the results are presented in Figure 4. On the one hand, for low friction numbers, $\mathrm{Re}_{\tau} < 100~(\mathrm{Re}_{\mathrm{b}} \leq 3 \times 10^3)$, the centreline velocity \overline{U}_{zc} approaches twice the bulk velocity \overline{U}_{zb} , which corresponds to the case of fully-developed laminar pipe flow. On the other hand, for $\mathrm{Re}_{\tau} \geq 5000$ in the fully-developed turbulent flow regime, $\overline{U}_{zc}/\overline{U}_{zb}$ decreases monotonically with a slight slope as the Reynolds number increases.

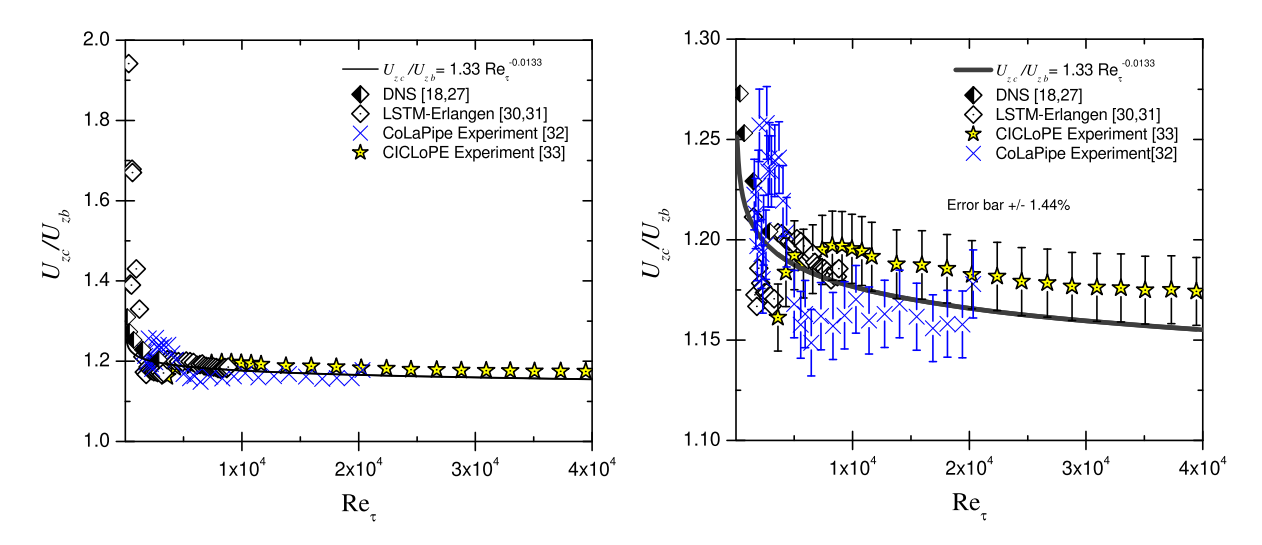


Figure 4. The centreline mean velocity \overline{U}_{zc} non-dimensionalised with the bulk velocity \overline{U}_{zb} from different pipe experiments for a wide range of the Reynolds numbers, (left) full range of data and (right) zoomed y-axis with $\pm 1.44\%$ an error bar.

The least-squares fit of the $\overline{U}_{zc}/\overline{U}_{zb}$ data measured in the CoLaPipe and CICLoPE facilities yields:

$$\frac{\overline{U}_{zc}}{\overline{U}_{zb}} = 1.33 \operatorname{Re}_{\tau}^{(-0.0133)} \tag{4}$$

Equation (4) reproduces $\overline{U}_{zc}/\overline{U}_{zb}$ with an uncertainty of $\pm 1.44\%$ for Re $_{\tau} \geq 5000$. It can also be expressed in terms of the centreline Reynolds number Re $_{c}$ as follows:

$$\frac{\overline{U}_{zc}}{\overline{U}_{zb}} = 1.404 \,\text{Re}_{c}^{(-0.0122)} \tag{5}$$

reproducing $\overline{U}zc/\overline{U}zb$ with a deviation of less than $\pm 1.19\%$.

An in-depth analysis of the centreline flow characteristics in terms of the two dimensionless numbers Re_c and Re_τ reveals a key outcome of this study. It is well known that the wall friction velocity u_τ is a crucial scaling parameter, requiring accurate and preferably independent measurements of the pipe wall friction [21]. It is common to express the wall friction, see Figure 2, in the form $\lambda = f(Re_b)$, where λ is the wall friction factor and Re_b is the bulk Reynolds number. Alternatively, the pipe wall friction data can be represented as a function of the centreline Reynolds number as illustrated in Figure 5.

The figure shows a unique correlation between the pipe wall friction, expressed in terms of Re_{τ} , and the centreline Reynolds number Re_c for a wide range of the Reynolds numbers $180 \le Re_{\tau} \le 5.5 \times 10^4$ (6889 $\le Re_c \le 3.7 \times 10^6$), which yields the following empirical relation:

$$Re_{\tau} = 0.048 Re_{c}^{0.923} \tag{6}$$

predicting the pipe wall friction with an accuracy of better than $\pm 2.06\%$. It is worth re-noting again that in Figure 5, the DNS data were obtained by Bauer et al. [18] and Bauer [27] in the Reynolds number range $180 \le Re_{\tau} \le 2880$ ($6889 \le Re_{c} \le 149,261$), the experimental data obtained using the CoLaPipe $3441 \le Re_{\tau} \le 17,608$ ($83,145 \le Re_{c} \le 9.185 \times 10^{5}$) and CICLoPE $10,847 \le Re_{\tau} \le 38,203$ ($634,363 \le Re_{c} \le 2.438 \times 10^{6}$) facilities. In addition, the pipe flow data extracted from Nikuradse [44] $3437 \le Re_{\tau} \le 55,500$ ($244,090 \le Re_{c} \le 3.6963 \times 10^{6}$) are shown. Thus, based on the data presented in Figure 5 and the empirical relation (6), one can predict the friction of the pipe with an accuracy better than $\pm 2.06\%$, simply, experimentally or numerically, via an accurate value for the local mean velocity at the pipe centreline \overline{U}_{zc} .

It is important to note that achieving a fully-developed turbulent state in pipe flow depends on several factors, including the design of the settling chamber, contraction geometry, inlet conditions (e.g. triggered or untriggered), flow velocity, pipe roughness and the pipe's length-to-diameter ratio. Nevertheless, once a fully developed turbulence state is established, Equation (6) and Figure 5 demonstrate remarkable robustness by



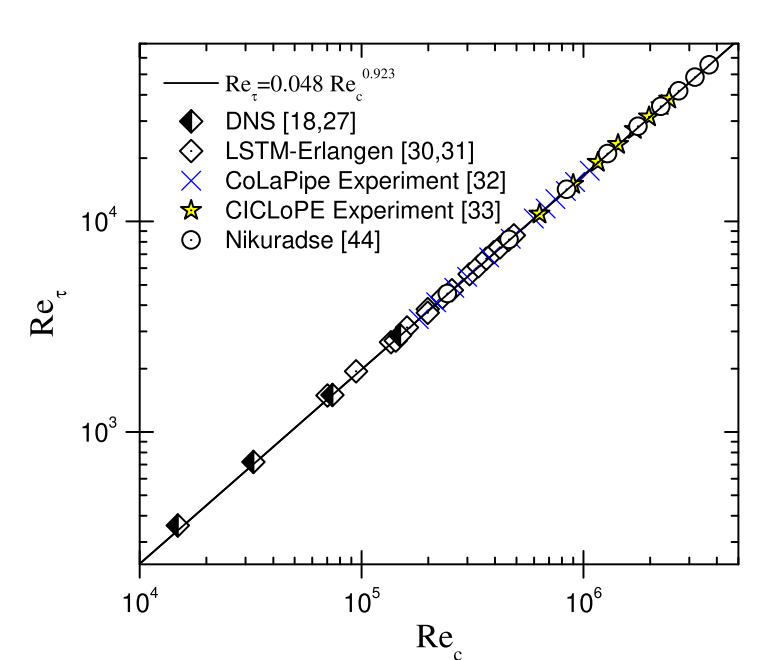


Figure 5. The development of the wall friction Reynolds number Re_{τ} = $u_{\tau}R/\nu$ as a function of the centreline-based Reynolds number Re_c for $180 \le \text{Re}_{\tau} \le 55 \times 10^3$ ($6886 \le \text{Re}_{c} \le 3.7 \times 10^6$), illustrating the proposed friction correlation, given by Equation (6).

predicting Re_τ directly from Re_c, regardless of the flow initiation conditions. This robustness is confirmed by consistent results results across a wide range of datasets, including those from the CICLOPE, CoLaPipe, and Erlangen pipe facilities, the classical experiments of Nikuradse [44], and recent DNS studies [18,27]. The strong agreement among these diverse sources highlights both the generality and the reliability of the proposed scaling relation, i.e. Equation (6).

Streamwise mean velocity profile

One of the main objectives of this manuscript is to analyze the streamwise mean velocity profile $\overline{U}_z = f(y)$ with particular emphasis on the inertial sublayer for friction Reynolds numbers in the range $180 \le \text{Re}_{\tau} \le$ 15,407, based on experimental and DNS data. The wall-normal coordinate pointing towards the pipe axis is denoted as y = (R - r). The scaling of the local mean velocity, $\overline{U}_z^+ = \overline{U}_z/u_\tau$, and the wall-normal distance, $y^+ = y/\ell_c$, was performed using the wall friction velocity $u_\tau = \sqrt{\tau_w/\rho}$ and the viscous length scale $\ell_c = \sqrt{\tau_w/\rho}$ ν/u_{τ} , respectively. The mean value of the wall friction is thus crucial for highlighting the effect of the friction Reynolds number, $\text{Re}_{\tau} = u_{\tau} \cdot R/\nu$, on the scaling laws. It is therefore not surprising that the friction Reynolds number significantly influences the mean velocity profile, given the dominance of either the viscous or inertial forces [4,21,45,46].

Given the significant influence of the friction Reynolds number on the mean velocity profile, it is important to examine how the velocity profile behaves in the inertial sublayer, in particular 'whether it follows a logarithmic or a power law' - an ongoing debate that has been explored in detail in several studies, including the early work of Millikan [47] and more recently Barenblatt [45] and Monkewitz and Nagib [46]. A so-called diagnostic function $\Xi = y^+ (dU_z^+/dy^+)$ is often used as a criterion to differentiate between the two laws, see e.g. Zanoun et al. [31], Österlund et al. [48] and Wosnik et al. [49]. Using $\Xi = f(y^+)$, Figure 6(a) examines whether the pipe mean velocity data follow a logarithmic behaviour. A constant behaviour of Ξ at sufficiently high Reynolds numbers leads to the existence of a logarithmic layer consistent with Millikan's [47] argument that a logarithmic law is expected in high Reynolds number turbulent channel and circular pipe flows, with a constant value of the von Kármán constant $\kappa = 1/\Xi$. Along the inertial sublayer in Figure 6(a), the Ξ -profiles exhibit a constant behaviour starting at $y^+ = 200 - 300$, indicating that 'the logarithmic law is a good representation of the mean velocity in the overlap region for Re_{τ} \geq 4500°. This is consistent with previous pipe

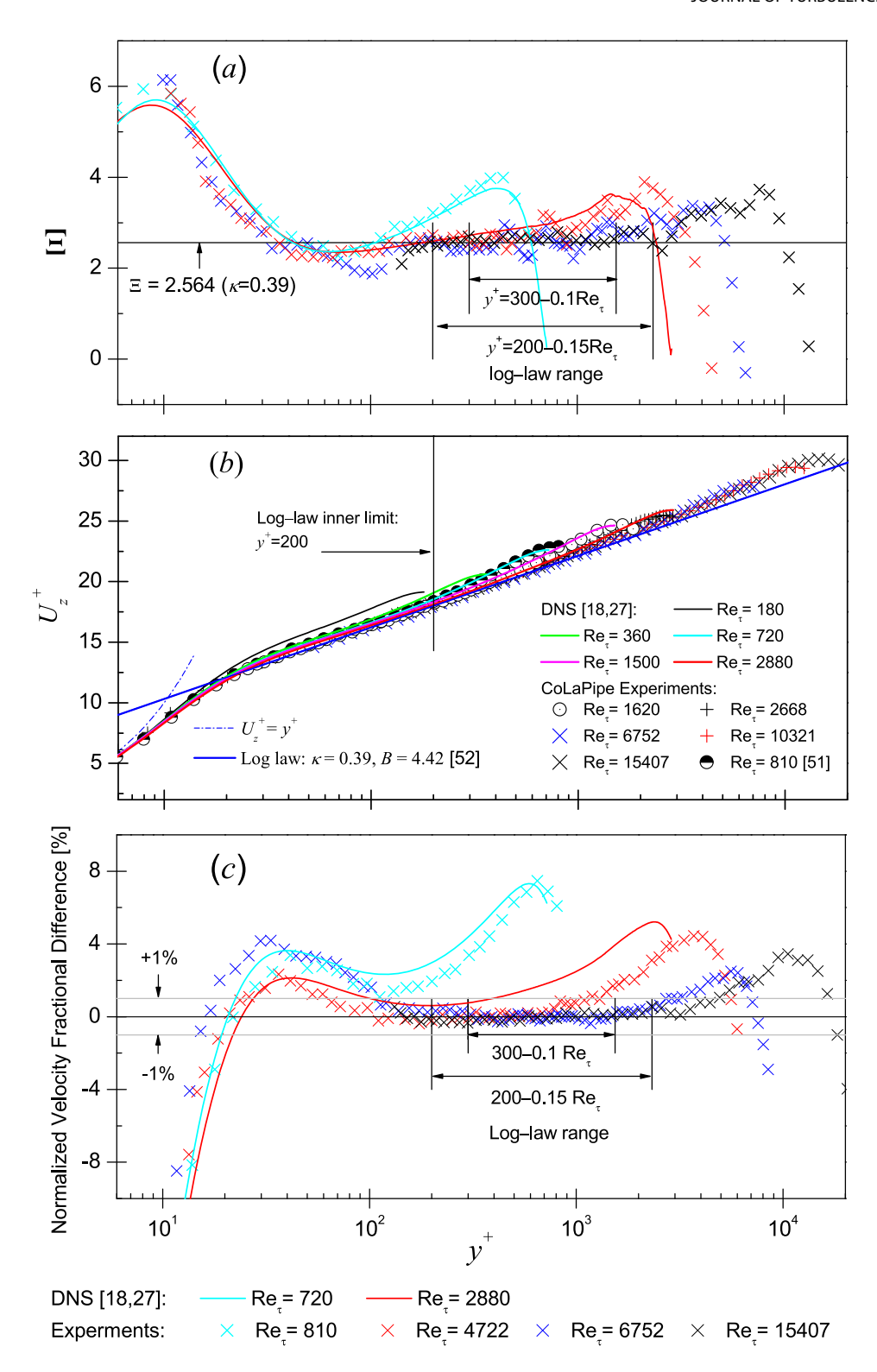


Figure 6. Inner scaling of the streamwise mean velocity $\overline{U}_{z}^{+} = f(y^{+})$ compared with the logarithmic velocity profile [50] in fully-developed turbulent pipe flow from experiments [21,31,51] and DNS [18,27].

flow studies by Zanoun [30] and Zanoun et al. [31] that further supports the logarithmic nature of the mean velocity profile.

Monkewitz and Nagib [46] recently concluded that it is not surprising that the inner-outer overlap limits of the logarithmic velocity profile are not fixed and remain a subject of ongoing debate; see also [9,13]. The present authors also emphasise that the overlap parameters, including the inner-outer limits of the logarithmic range and the slope of the logarithmic line, depend on the resolution of the measurement technique, the accuracy of the mean velocity and the wall friction data. The present hot-wire results, along with all of the first author's previous data, support $y^+ = 200 - 300$ as an appropriate inner limit for the logarithmic range, as shown in Figure 6(a). Figure 6(b) shows the logarithmic mean velocity profile [50]:

$$\overline{U}_z^+ = \frac{1}{\kappa} \ln y^+ + B \tag{7}$$

where κ is the von Kármán constant and B is the additive constant. The logarithmic line with $\kappa=0.39$ and B=4.42 [52] represents accurately the mean velocity profiles for $\text{Re}_{\tau} \geq 4500$ along the wall layer, with $200 \leq y^+ \leq 0.15\text{Re}_{\tau}$. Although some recent studies, such as those by Nagib and Chauhan [10] and Monkewitz and Nagib [46], suggest values of $\kappa=0.41$ and B=5.0, the authors chose to use the log-law constants proposed by Perry et al. [52], namely $\kappa=0.39$ and B=4.42. This choice is based on the fact that the data presented in Figures 6(a,b) align well with Perry et al. [52] logarithmic line. The mean velocity profiles plotted in Figure 6(b) cover two ranges of the Reynolds numbers: experimental data for $810 \leq \text{Re}_{\tau} \leq 15,407$ and DNS data for $180 \leq \text{Re}_{\tau} \leq 2880$ [18,27]. The measured velocity profiles for $810 \leq \text{Re}_{\tau} \leq 15,407$, presented in Figure 6(b), are based on ensemble-averaged laser-Doppler anemometry (LDA) and hot-wire data. Note that the mean velocity profile for $\text{Re}_{\tau} = 810$ is extracted from [51] and was obtained using the LDA. The DNS mean velocity profiles data were obtained by averaging the streamwise velocity component for $180 \leq \text{Re}_{\tau} \leq 2880$ [18,27].

The experimental profiles shown in Figure 6(b) for low Reynolds numbers $Re_{\tau} \le 2 \times 10^3$ collapse near the wall in alignment with the DNS data. The figure also shows data collapse along the overlap region, following the logarithmic velocity profile for $Re_{\tau} \ge 4.5 \times 10^3$. However, only the high Reynolds number DNS case, i.e. $Re_{\tau} = 2880$, exhibits a logarithmic behaviour along the log range $y^+ = 200 - 432$.

To examine how well the current experimental and numerical data align with the logarithmic line proposed by Perry et al. [52], the so-called normalised velocity fractional difference is used. This is defined as $\Delta \overline{U}_z^+ = (\overline{U}_z^+)_{predicted} - \overline{U}_z^+$ calculated and presented in 6(c). In this expression, \overline{U}_z^+ predicted is calculated using the logarithmic velocity profile with Perry's recommended constants $\kappa = 0.39$ and B = 4.42. Figure 6(c) shows that the deviation of the selected experimental velocity data from the logarithmic velocity profile is minimal for wall-normal distances $200 \le y^+ \le 0.15 \mathrm{Re}_\tau$, where the velocity closely matches the logarithmic line. Along the logarithmic range, for sufficiently high Reynolds numbers ($\mathrm{Re}_\tau \ge 4500$), the measured velocity closely follows the logarithmic line, indicating the high accuracy of the present data. The deviation of two selected DNS cases, [18,27], for $\mathrm{Re}_\tau = 720$ and $\mathrm{Re}_\tau = 2880$, from the logarithmic velocity is also shown in Figure 6(c). A large deviation is observed for $\mathrm{Re}_\tau = 720$, as this case is far from behaving logarithmically. In contrast, the deviation for $\mathrm{Re}_\tau = 2880$ lies within $\pm 1\%$ along the wall distance $y^+ = 200 - 432$, indicating reasonable logarithmic behaviour.

Streamwise velocity fluctuations

The wide range of turbulence scales in pipe flow makes spanwise-spatial resolutions of hot-wire probe and grid spacing critical for accurate measurements and simulations near the wall. Spanwise-spatial resolution is especially important, where steep velocity gradients and strong shear significantly affect higher-order turbulence statistics [4,6,25,53,54]. To account for finite probe size, Smits et al. [53] proposed a spatial correction for the streamwise Reynolds stress $\langle u_z'^2 \rangle^+$ based on the attached eddy hypothesis, which is valid over a wide range of Reynolds numbers and wire lengths $0 < \ell_{hw}^+ < 150$. Notably, this correction has been successfully applied to the present hot-wire data shown in Figure 7 and Appendix. Figure 7(a) compares the uncorrected and corrected $\langle u_z'^2 \rangle^+$ profiles for two cases: $\text{Re}_{\tau} = 2687 \ (\ell_{hw}^+ = 45.5)$ and $\text{Re}_{\tau} = 15,407 \ (\ell_{hw}^+ = 203)$. A clear dependence of $\langle u_z'^2 \rangle^+$ on probe length is observed in the near-wall region, with a sharp drop near $y^+ \approx 15$ due to spanwise spatial averaging along the hot-wire length. This attenuation, caused by insufficient spatial resolution, persists for approximately $y^+ \leq 0.1\text{Re}_{\tau}$ where the motion at all turbulence scales is highly anisotropic, see e.g. [25], and beyond which its effect becomes negligible. One may therefore conclude that resolution issues are irrelevant in the core region, where the characteristic length scales–governed by the Taylor microscale–are significantly larger than those near the wall. As shown in Figure 7(a), the correction is

therefore unnecessary beyond the outer edge of the log layer $y^+ \ge 0.15 \text{Re}_{\tau}$. Consequently, the centreline turbulence intensity $\langle u_z'^2 \rangle^{1/2}/\overline{U}_{zc}$, shown in Figure 3, remains unaffected by probe resolution–consistent with Ligrani and Bradshaw [25], who noted also that attenuation decreases with distance from the wall as eddy sizes increase.

To demonstrate the effectiveness of the spatial correction adopted, the two experimental cases at Re_{τ} = 2687 and Re_{τ} = 15,407 were corrected and plotted alongside their uncorrected counterparts in Figure 7(a). Although the correction technique by Smits et al. [53] is formally limited to wire lengths $\ell_{hw}^+ \leq 150$, it was applied to the case of $\text{Re}_{\tau} = 15,407$ ($\ell_{hw}^+ = 203$) and still showed good performance. The corrected profiles, in particular, for $Re_{\tau} = 2687$, show significantly improved agreement with expected near-wall behaviour, confirming the impact of the probe resolution. As discussed in Appendix, accurate comparisons between DNS at Re_{τ} = 2880 [18,27] and hot-wire measurements Re_{τ} = 2687 in Figure 7(a) validate the effectiveness of the correction method adopted from Smits et al. (2011), applied even in the range $30 < y^+ < 100$. However, in the viscous sublayer v^+ < 30, the corrections become more sensitive due to steep small-scale gradients, leading to some deviations from the DNS data.

Based on all hot-wire lengths summarised in Table I, the spatial correction method by Smits et al. [53] was applied to account for spanwise-resolution limitations. The corrected streamwise Reynolds stress data $\langle u_z'^2 \rangle^+$ for $1620 \le \text{Re}_{\tau} \le 15,407$ are presented in Figure 7(b) alongside DNS results for $180 \le \text{Re}_{\tau} \le 2880$ [18,27]. Near the wall, the corrected profiles align well with DNS and show a distinct Reynolds-number-dependent inner peak around $y^+ \approx 15$, consistent with findings in [17]. This observed dependence supports the view that the inner peak reflects interactions between near-wall and outer-layer motions [13,55], rather than being an artifact of probe resolution [6]. The present results also agree with the empirical formulation by Hutchins et al. [54] and experimental data from [9]. Notably, the inner peak consistently occurs near the location of maximum turbulent kinetic energy production, as reported in [11,56,57].

Beyond the inner limit of the logarithmic region, $y^+ = 200$, a plateau in $\langle u_z'^2 \rangle^+$ is clearly visible along the overlap region, possibly resulting from a constant behaviour of the Reynolds shear stress $\langle u'_z u'_r \rangle^+$ in the logarithmic region for the high Reynolds number cases $6752 \le \text{Re}_{\tau} \le 15,407$ [57]. The plateau observed could be a result of structural changes related to the outer flow phenomena postulated in [9]. However, an outer peak is barely observable in Figure 7(b), which might be due to insufficiently high Reynolds numbers achieved in the present study in contrast to [17] who obtained it for $Re_{\tau} \geq 20,000$.

At high Reynolds numbers, Townsend [2] claimed a logarithmic decay for the streamwise Reynolds stress $\langle u_z^2 \rangle^+$ along the inertial sublayer, expressed as:

$$\left\langle u_{z}^{\prime 2}\right\rangle ^{+}=B_{2}-A_{2}\ln(y^{+}/\mathrm{Re}_{\tau}),$$
 (8)

where A_2 and B_2 are Reynolds number dependent constants. Hultmark [58] and Hultmark et al. [59] confirmed Townsend's logarithmic decay of the streamwise normal stress $\langle u_z'^2 \rangle^+$, as expressed above in Equation (8). They proposed constants $A_1 = 1.25$ [58] or $A = 1.24 \pm 0.1$ [59] and $B_1 = 1.61$ [59] or B = 1.61 1.48 ± 0.3 [59] for smooth pipe flow at high Reynolds numbers. In Figure 7(b), the data for Re_{τ} = 15,407 exhibit a logarithmic decay in $\langle u_z'^2 \rangle^+$ within the limited wall-normal range 0.065 $< y^+/\text{Re}_\tau < 0.15$, showing good agreement with Equation (8) when using the constants $A_1 = 1.25$ and $B_1 = 1.61$ adopted from [58,59].

To explore alternative representations of the streamwise normal stress $\langle u_z^2 \rangle^+$ in the region beyond the inner layer, including the overlap region, Nagib et al. [60] proposed a quarter-power law over the wall-normal distance 0.3 < Y < 0.7 for $Re_{\tau} > 2000$, expressed in the form:

$$\phi(Y) = \alpha_{\phi} - \beta_{\phi} Y^{-1/4},\tag{9}$$

where $\phi(Y) = \langle u_z'^2 \rangle^+$ and $Y = y^+/\text{Re}_\tau$. This functional form has been observed to capture the general shape of the stress profile across a broader wall-normal range in high-fidelity datasets.

Two selected cases of $\phi(Y) = \langle u_z^2 \rangle^+$ – DNS at Re_{\tau} = 2880 and experiment at Re_{\tau} = 15,407 – are shown in Figure 7(c). A closer examination of these cases in Figure 7(c) reveals that within the wall-layer range 0.3 < Y< 0.7, as proposed by Nagib et al. [60], the logarithmic and quarter-power laws yield nearly indistinguishable results. Nevertheless, both formulations, i.e. power versus log laws, provide valuable insights for modelling the

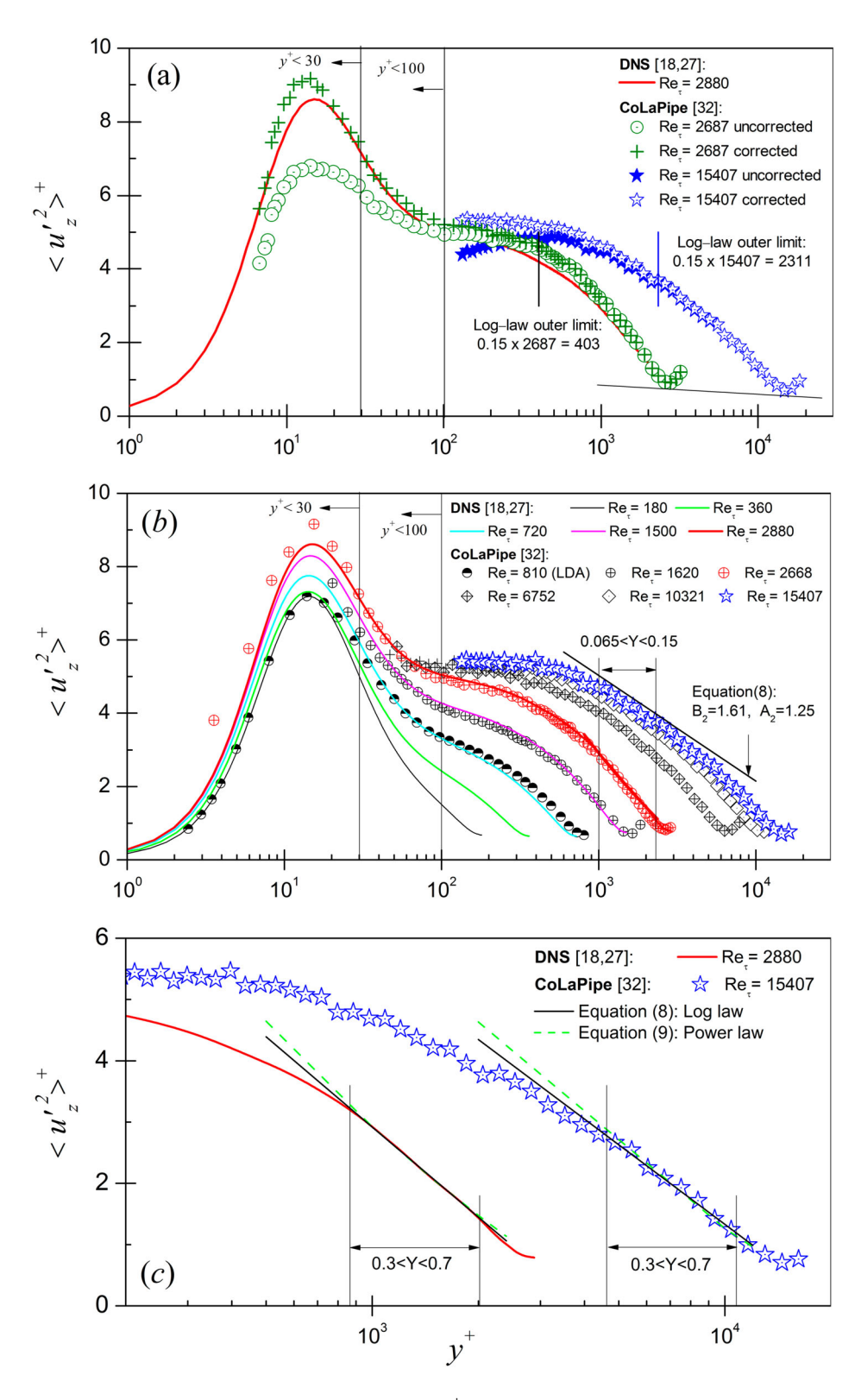


Figure 7. Inner scaling of the streamwise Reynolds stress $\langle u_z'^2 \rangle^+$ in fully-developed turbulent pipe flow from experiments [21,31,51] and DNS [18,27], The region $y^+ < 30$ indicates where hot-wire data are affected by spatial resolution limitations, as detailed in Appendix. Vertical lines for each Re $_{\tau}$ in (c) represent the contrast between the logarithmic and the 1/4-power law trends, note that $Y=y^+/{\rm Re}_{\tau}$. Equation (8) constants– DNS (Re $_{\tau}=2880$): $B_2=0.6736$, $A_2=2.1222$, Exp. (Re $_{\tau}=15,407$): $B_2=0.5205$, $A_2=1.8736$ and Equation (9) constants– DNS (Re $_{\tau}=2880$): $\alpha_{\phi}=-6.177$, $\beta_{\phi}=-6.986$, Exp. (Re $_{\tau}=15,407$): $\alpha_{\phi}=-5.5187$, $\beta_{\phi}=-6.153$.

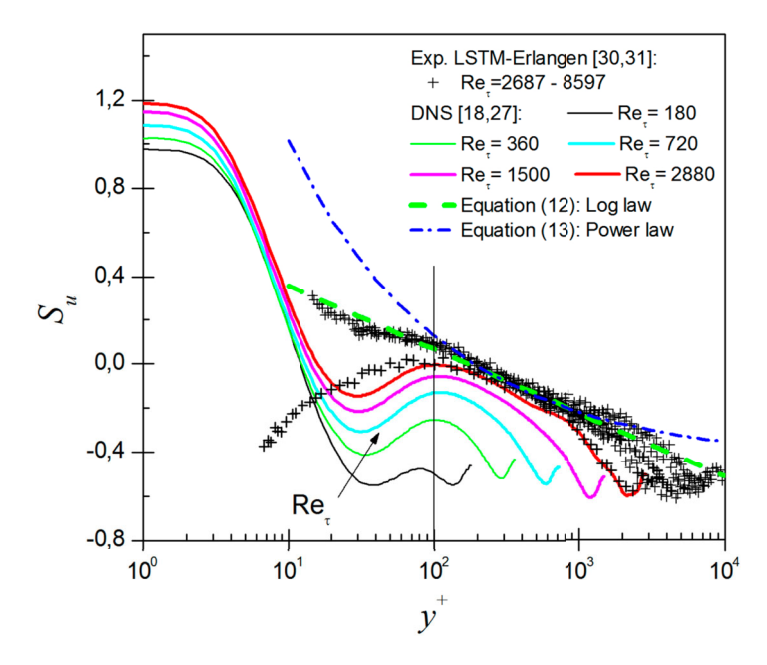


Figure 8. Present experimental streamwise skewness S_u in pipe flow, uncorrected for spanwise-spatial resolution effects, compared to DNS data [18,27] for a relatively wide range of Reynolds numbers. The arrow indicates increasing friction Reynolds number Re_{τ} .

streamwise Reynolds stress, with their effectiveness potentially influenced by factors such as flow configuration, Reynolds number, and the extent of the wall-normal domain considered. While the logarithmic relation may serve as a local approximation in specific regions, the quarter-power law provides an alternative with potentially broader applicability. In this context, Equation (8) is retained for comparison purposes. It should be noted that the slopes of the logarithmic lines in Figure 7(c) differ from those in Figure 7(b). Continued analysis is underway to determine the conditions under which each formulation most accurately represents the data.

Skewness and flatness factors

Additional focus is being directed to the third and fourth moments—skewness and flatness factors. Both of these moments provide valuable insights into the spatio-temporal distribution of the streamwise velocity fluctuations around the mean and are crucial for understanding the structure of pipe flow. While even-numbered moments are always positive, third and higher odd-numbered moments retain sign information, providing important statistical details about coherent structures [4]. The skewness and flatness factors of the streamwise velocity fluctuations are commonly defined as follows:

$$S_u = \langle u_z^{\prime 3} \rangle / \langle u_z^{\prime 2} \rangle^{3/2}, \tag{10}$$

$$F_u = \langle u_z^{\prime 4} \rangle / \langle u_z^{\prime 2} \rangle^2. \tag{11}$$

The distributions of both S_u and F_u , obtained numerically and experimentally, are shown in Figures 8 and 9, respectively, for friction Reynolds numbers in the range $180 \le \text{Re}_\tau \le 8597$. Notably, S_u and F_u from measurements were obtained without corrections for the effects of spanwise spatial resolution on the hot-wire data, particularly near the wall. Thus, the effect of Reynolds number in the viscous sublayer could not be addressed with the present experimental data due to the insufficient resolution of the hot-wire probe. It is observed that S_u is influenced by probe size for $y^+ \le 200$, compared to $y^+ \le 30$ for F_u , consistent with [61]. The DNS results by Bauer et al. [18] and Bauer [27] were thus used to provide better insights into the physical behaviour of S_u and F_u near the wall. A near-wall dependence of the DNS streamwise skewness, visible in Figure 8, is likely due to the interaction of very large-scale motions in the core region with small-scale motions [18,27].

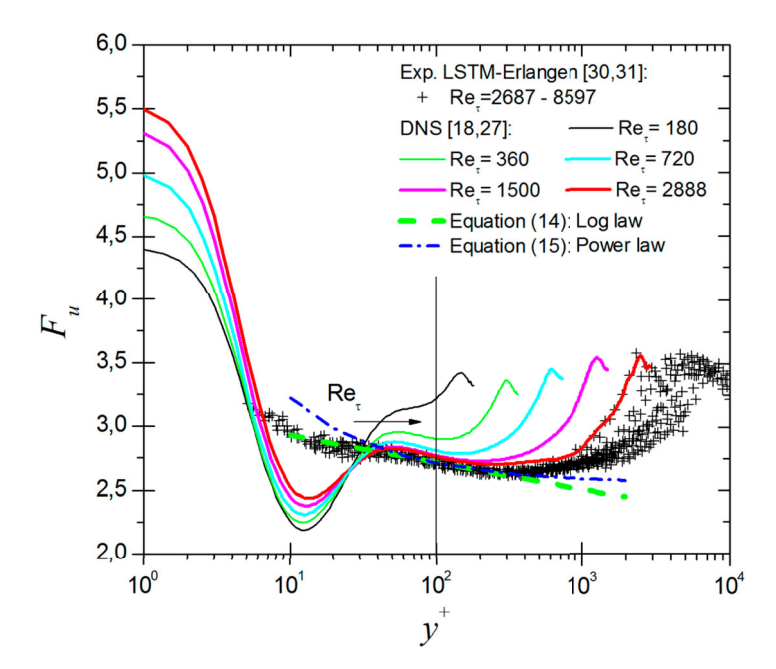


Figure 9. Experimental streamwise flatness F_u in pipe flow, uncorrected for spatial resolution effects, compared to DNS data [18,27] for a relatively wide range of Reynolds numbers. The arrow indicates increasing friction Reynolds number Re_{τ}.

Near-wall turbulence is characterised by small scales, which, along with inhomogeneity and anisotropy, deviate significantly from a Gaussian distribution. For Gaussian signals, the expected values for the skewness and flatness factors are $S_u = 0$ and $F_u = 3$, respectively. The deviation of S_u from zero, observed in Figure 8, indicates a degree of temporal asymmetry in the streamwise velocity fluctuations, reflecting phenomena such as acceleration versus deceleration, or sweep versus ejection events [4]. On the other hand, a deviation of F_u from 3, as shown in Figure 9, indicates a peaky signal, commonly associated with intermittent turbulent events near the wall [4].

Near the wall, $y^+ \le 5$, the DNS data [18,27] in Figures 8 and 9 show a clear Reynolds number-dependence of both skewness and flatness factors, respectively. The DNS S_u data predominantly show positive values within the wall-normal sublayer $y^+ \le 10$, reflecting a dominance of sweeping events. In contrast, for $y^+ > 10$, negative S_u values are observed, consistent with ejection events [4]. A distinct S_u Reynolds-dependence is also seen for $y^+ \ge 10$ with a prominent local minimum at a wall-normal distance around $y^+ \approx 33$ across all DNS Reynolds number cases. A second local minimum of S_u appears at the pipe centreline, reaching an asymptotic value of $S_u \approx -0.5$ for Reynolds numbers $Re_\tau \ge 1500$ in good agreement with the experimental data.

For $y^+ \ge 200$, the S_u experimental data for $Re_\tau = 2687$ show satisfactory agreement with the high Reynolds number $Re_\tau = 2880$ DNS data [18,27]. In the overlap region, S_u exhibits a logarithmic behaviour with no dependence on the Reynolds number for $Re_\tau > 1500$. The DNS data for $Re_\tau = 2880$, along with experiments for $2687 \le Re_\tau \le 8597$, show S_u to collapse along the logarithmic layer. Considering the DNS data for $Re_\tau = 2880$ and all experimental data presented in the wall-normal distance range $200 \le y^+ \le 0.15Re_\tau$, the streamwise skewness can be fitted either logarithmically or using a power law. The logarithmic expression, indicated by the gray-dashed line in Figure 8, reads:

$$S_u = -0.126 \ln(y^+) + 0.647$$
, for $200 \le y^+ \le 0.15 \text{Re}_{\tau}$, (12)

whereas the power law is fitted as:

$$S_u = -0.438 + 3.74(y^+)^{-0.41}, \text{ for } 200 \le y^+ \le 0.15 \text{Re}_{\tau},$$
 (13)

indicated by the blue-dashed line in Figure 8. In the fitted data range, the root mean square error of the logarithmic relation is 0.023, comparable to an error of 0.022 for the power law.

In Figure 9, the DNS data show a Reynolds-number dependence of F_u , with higher values close to the pipe wall and an asymptotic value of $F_u \approx 3.5$ at the pipe centreline for Re_{τ} \geq 1500, matching a value for

isotropic and homogeneous turbulence [4,43]. At $y^+ \approx 15$, F_u reaches a minimum and exhibts Reynolds number-dependence while S_u is approximately zero for $\text{Re}_{\tau} \geq 1500$. This location, i.e. $y^+ \approx 15$, coincides with the peak of the streamwise Reynolds stress $(u_z^2)^+$, see Figure 7 and the peak of the turbulent kinetic energy production [11,56,57]. The Reynolds-number effect on F_u is evident in the core region, similar to the corresponding Reynolds-number effects on S_u illustrated in Figure 8. The Reynolds number dependence of F_u observed might be attributed to a diminished stretching of the vorticity further away from the wall [6] or to the large-scale inactive motion [9,62].

Similarly, the flatness factor profile F_u collapses well and shows Reynolds number-independence for Re₇ \geq 1500 at the onset of the logarithmic layer. The collapse of the F_u -profiles for $50 \le y^+ \le 300$ and $Re_\tau > 1500$ depicted in Figure 9 can be fitted with the logarithmic relation:

$$F_{\nu} = -0.092 \ln(y^{+}) + 3.14, \quad \text{for } 50 \le y^{+} \le 300,$$
 (14)

or the power law:

$$F_u = 2.547 + 2.76(y^+)^{-0.61}, \text{ for } 50 \le y^+ \le 300,$$
 (15)

respectively. For the streamwise flatness, the logarithmic expression estimates the data with a root mean square error of 0.020, compared to 0.019 for the power law. Consequently, for the present data set, a logarithmic law and a power law yield comparable results. Note that we estimated the error induced by insufficient resolution of the HWA probe near the wall using filtered DNS data, see Appendix. For $Re_{\tau} = 2880$, we found an error of less than $\pm 2\%$ of the corresponding maximum value at wall distances above $y^+ = 100$ for the streamwise skewness and $y^+ = 20$ for the streamwise flatness. However, since this error might increase for higher Reynolds number data, particularly near the wall, there remains some uncertainty in the near-wall end of the high-Reynolds number profiles in Figure 8 and 9.

4. Conclusions and final remarks

High-quality experimental and numerical data for fully developed turbulent pipe flows have been presented and discussed over a wide range of friction Reynolds numbers $180 \le \text{Re}_{\tau} \le 55 \times 10^3$. The data addressed several key open issues in pipe flow pointed out in the introduction, focussing on the effects of Reynolds number on turbulence statistics, with particular emphasis on the centreline turbulence quantities and pipe wall friction. A unique friction relation, $Re_{\tau} = 0.048 Re_c^{0.923}$, is proposed, which predicts the pipe wall friction with an accuracy of better than $\pm 2.06\%$ over a broad Reynolds number range. Let us compare our new friction relation with some classical friction factor laws. First, the Blasius (1913) relation, $\lambda = 0.3164 \, \text{Re}_h^{-0.25}$, is semi-empirical, valid only for $Re_b \leq 10^5$, and does not directly relate to the centreline Reynolds number Re_c . Second, Nikuradse's [44] historical data remain pivotal but resulted from detailed mean-pressure-gradient measurements and bulk velocity estimation. Third, the friction relation by McKeon et al. [63], $1/\sqrt{\lambda}$ $1.930 \log \text{Re}_b \sqrt{\lambda} - 0.537$, covers a wide Reynolds number range, relying on precise streamwise mean-pressure gradient and bulk velocity data, however, it is implicit, which may limit its applicability in some experimental contexts. In contrast, our correlation is explicit, which enables accurate wall-friction prediction using only a single-point measurement at centreline, \overline{U}_{zc} , obtained experimentally or numerically, without reliance on near-wall measurements, mean-pressure-gradient data, or facility-specific calibration.

Using the local centreline mean velocity as an appropriate integral velocity scale in the core region, the paper provides an interpretation for the monotonic decrease in centreline streamwise turbulence intensity $\langle u_z'^2 \rangle^{1/2}/\overline{U}_{zc}$ as the Reynolds number Re_c increases based on a thorough analysis of the streamwise meanmomentum equation. For sufficiently high friction Reynolds number $Re_{\tau} \ge 4.5 \times 10^3$, the inner scaling of the present streamwise mean velocity profiles aligns with the logarithmic profile with $\kappa = 0.39$ and B = 4.42as proposed by Perry et al. [52].

Significant attenuation in hot-wire signals due to spatial averaging occurs for $y^+ \le 0.1$, which necessitates corrections in this region [53]. However, beyond $y^+ = 0.1$, the resolution effects become negligible and the uncorrected data remain reliable. The correction method by Smits et al. [53], even when applied beyond its applicable limit ($\ell_{hw}^+ \le 150$), improves the agreement of hot-wire data with DNS and reveals a consistent inner peak near $y^{+}\approx 15$, confirming that this peak is a physical feature rather than a measurement artifact.

Additionally, both Townsend's logarithmic law and Nagib et al.'s quarter-power law effectively capture the decay of streamwise Reynolds stress $\langle u_z^2 \rangle^+$ at high Reynolds numbers. While they yield similar results in the range 0.3 < Y < 0.7, the quarter-power law may offer broader applicability. The comparison of higher-order statistics, i.e. skewness and flatness, between experiments and DNS highlights that spatial resolution limits in the measurements mainly affect the near-wall region, while in the logarithmic layer and core region, both datasets show excellent agreement for Re_{τ} \geq 2880. In this high- Re_{τ} regime, the skewness and flatness collapse to Reynolds-number-independent profiles that can be described with equal accuracy by either logarithmic or power-law correlations.

Further analysis of the streamwise mean velocity profiles as well as the streamwise Reynolds stress in light of the recent work of Monkewitz and Nagib [46] and [60,64,65] is planned for a separate publication. Further collaboration with the University of Bologna, utilising the CICLOPE facility, is planned, alongside the use of NSTAP probes at the CoLaPipe in cooperation with Alex Smits from Princeton University. Additionally, collecting precise near-wall experimental data on skewness and flatness will be crucial for assessing the grid dependence of near-wall skewness and flatness values, providing valuable insights for improving the accuracy of numerical simulations in near-wall turbulent flows at high Reynolds numbers.

Acknowledgments

The authors gratefully acknowledge the scientific support and HPC resources provided by the German Aerospace Center (DLR). The HPC system CARA is partially funded by "Saxon State Ministry for Economic Affairs, Labour and Transport" and "Federal Ministry for Economic Affairs and Climate Action". The HPC system CARO is partially funded by "Ministry of Science and Culture of Lower Saxony" and "Federal Ministry for Economic Affairs and Climate Action".

Data availability statement

The data that support the findings of this study are available from the corresponding author, [E.-S. Zanoun], upon reasonable request.

Disclosure statement

The authors declare that they have no known competing financial interests or personal relationships that could have appeared to influence the work reported in this paper.

Funding

This project is funded within the DFG-Priority Programme 1881 "Turbulent Superstructures," grant nos. EG100/24-1 & EG100/24-2. Support received from the RI-funding of European High performance Infrastructures in Turbulence (EUHIT) for measurement campagin at CICLoPE, University of Bologna, is appreciated.

ORCID

El-Sayed Zanoun http://orcid.org/0000-0003-3834-1348

References

- [1] Laufer J. The structure of turbulence in fully-developed pipe flow. Nat Adv Comm Aero. 1953;1174:1-18.
- [2] Townsend AA. The structure of turbulent shear flow. Cambridge, UK: Cambridge University Press; 1976.
- [3] Perry AE, Abell CJ. Scaling laws for pipe-flow turbulence. J Fluid Mech. 1975;67:257–271. doi: 10.1017/S002211 2075000298
- [4] Gad-el-Hak M, Bandyopadhyay PR. Reynolds number effects in wall-bounded turbulent flows. Appl Mech Rev. 1994;47:307-365. doi: 10.1115/1.3111083
- [5] Kim J, Moser R. Turbulence statistics in fully-developed channel flow at low Reynolds number. J Fluid Mech. 1987;177:133–166. doi: 10.1017/S0022112087000892
- [6] Wei T, Willmarth WW. Reynolds number effects on the structures of a turbulent channel flow. J Fluid Mech. 1989;204:57-95. doi: 10.1017/S0022112089001667
- [7] Durst F, Jovanovic J, Sender J. LDA measurements in the near-wall region of a turbulent pipe flow. J Fluid Mech. 1995;295:305-335. doi: 10.1017/S0022112095001984
- [8] Mochizuki S, Nieuwstadt FTM. Reynolds-number-dependence of the maximum in the streamwise velocity fluctuations in wall turbulence. Exp Fluids. 1996;21:218-226. doi: 10.1007/BF00191694



- [9] Morrison JF, McKeon BJ, Jiang W, et al. Scaling of the streamwise velocity component in turbulent pipe flow. J Fluid Mech. 2004;508:99-131. doi: 10.1017/S0022112004008985
- [10] Nagib H, Chauhan K. Variations of von kármán coefficient in canonical flows. Phys Fluids. 2008;20:418–428. doi: 10.1063/1.3006423
- [11] Hultmark MN, Bailey SC, Smits A. Scaling of near-wall turbulence in pipe flow. J Fluid Mech. 2010;694:103-113. doi: 10.1017/S0022112009994071
- [12] Marusic I, Mathis R, Hutchins N. High Reynolds number effects in wall turbulence. Int J Heat Fluid Flow. 2010;31:418-428. doi: 10.1016/j.ijheatfluidflow.2010.01.005
- [13] Marusic I, McKeon BJ, Monkewitz PA, et al. Wall-bounded turbulent flows at high Reynolds numbers: recent advances and key issues. Phys Fluids. 2010;22:1-24. doi: 10.1063/1.3453711
- [14] Smits AJ, McKeon BJ, Marusic I. High-Reynolds number wall turbulence. J Annu Rev Fluid Mech. 2011;43:353–375. doi: 10.1146/fluid.2011.43.issue-1
- [15] Alfredsson PH, Segalini A, Örlü R. A new scaling for the streamwise turbulence intensity in wall-bounded turbulent flows and what it tells us about the "outer" peak. Phys Fluids. 2011;23:041702. doi: 10.1063/1.3581074
- [16] Keirsbulck L, Fourrié G, Labraga L, et al. Scaling of statistics in wall-bounded turbulent flows. C R Mecanique. 2006;340:420-433. doi: 10.1016/j.crme.2012.02.005
- [17] Willert WC, Soria J, Stanislas M, et al. Near-wall statistics of a turbulent pipe flow at shear Reynolds numbers up to 40,000. J Fluid Mech. 2017;826:R5. doi: 10.1017/jfm.2017.498
- Bauer C, Feldmann D, Wagner C. On the convergence and scaling of high-order statistical moments in turbulent pipe flow using direct numerical simulations. Phys Fluids. 2017;29:125105. doi: 10.1063/1.4996882
- [19] Pirozzoli S, Romero J, Fatica M, et al. One-point statistics for turbulent pipe flow up to $Re_{\tau} \approx 6000$. J Fluid Mech. 2021;926:A28. doi: 10.1017/jfm.2021.727
- [20] Monkewitz PA. The late start of the mean velocity overlap log law at $y^+ = o(10^3)$ a generic feature of turbulent wall layers in ducts. J Fluid Mech. 2021;910:A45. doi: 10.1017/jfm.2020.998
- [21] Zanoun E-S, Egbers C, Nagib H, et al. Wall friction relations in wall-bounded shear flows. Euro J Mech B/Fluids. 2021;89:171-179. doi: 10.1016/j.euromechflu.2021.03.007
- [22] Yao J, Rezaeiravesh S, Schlatter P, et al. Direct numerical simulations of turbulent pipe flow up to Re_{τ} \approx 5200. J Fluid Mech. 2023;956:A18. doi: 10.1017/jfm.2022.1013
- [23] Zanoun E-S, Dewidar D, Egbers C. Reynolds number dependence of azimuthal pipe flow structure. J Fluid Mech. 2023;973: A1. doi: 10.1017/jfm.2023.700
- [24] Johansson AV, Alfredsson PH. Effects of imperfect spatial resolution on measure ment of wall-bounded turbulent shear flows. J. Fluid Mech. 137, 409. J Fluid Mech. 1983;122:295-314-doi: 10.1017/S0022112082002225
- [25] Ligrani PM, Bradshaw P. Subminiature hot-wire sensors: development and use. Phys E Sci Instrum. 1987;20:323-332-doi: 10.1088/0022-3735/20/3/019
- [26] Örlü R, Alfredsson PH. On spatial resolution issues related to time-averaged quantities using hot-wire anemometry. Exp Fluids. 2010;49:101-110. doi: 10.1007/s00348-009-0808-1
- [27] Bauer C. Direct numerical simulation of very-large-scale motions in turbulent pipe flow [Ph.d. thesis]. Technische Universität Ilmenau; 2021.
- [28] Wei T, Fifer P, Klewicki J, et al. Properties of the mean momentum balance in turbulent boundary layer, pipe and channel flows. J Fluid Mech. 2005;522:303-327. doi: 10.1017/S0022112004001958
- [29] Panton RL. Composite asymptotic expansions and scaling wall turbulence. Philos Trans R Soc A. 2007;522:733-754. doi: 10.1098/rsta.2006.1951
- [30] Zanoun E-S. Answers to some open questions in wall-bounded laminar and turbulent shear flows [Ph.d. thesis]. Universität Erlangen-Nürnberg; 2003.
- [31] Zanoun E-S, Durst F, Bayoumi O, et al. Wall skin friction and mean velocity profiles of fully-developed turbulent pipe flows. J Exp Therm Fluid Sci. 2007;32:249-261. doi: 10.1016/j.expthermflusci.2007.04.002
- König F, Zanoun E-S, ÖngÜner E, et al. The colapipe-the new cottbus large pipe test facility at brandenburg university of technology cottbus-senftenberg. J Rev Sci Instrum. 2014;85:075115. doi: 10.1063/1.4884717
- [33] Fiorini T. Turbulent pipe flow high resolution measurements in CICLoPE [Ph.D. thesis]. Universita Di Bologna; 2017.
- [34] McKeon BJ, Zagarola MV, Smits AJ. A new friction factor relationship for fully-developed pipe flow. J Fluid Mech. 2005;538:429-443. doi: 10.1017/S0022112005005501
- [35] Nagib HM, Chauhan KA, Monkwetiz PA. Approach to an asymptotic state for zero pressure gradient turbulent boundary layers. Phil Trans R Soc A. 2007;365:755-770. doi: 10.1098/rsta.2006.1948
- [36] Örlü R, FranssonJens JHM, Alfredson FH. On near wall measurements of wall bounded flows-the necessity of an accurate determination of the wall position. Prog Aerosp Sci. 2010;46:353-387. doi: 10.1016/j.paerosci.2010.04.002
- [37] Bradshaw P. An introduction to turbulence and its measurement. Oxford (NY): Pergamon Press; 1971.
- [38] Bruun HH. Hot-wireanemometry. New York: Oxford University Press; 1995.
- [39] Shaw R. The influence of hole dimensions on static pressure measurements. J Fluid Mech. 1960;7:550-564. doi: 10.1017/S0022112060000281
- [40] Tennekes HA, Lumley JL. Firstcourse inturbulence. M.I.T. Press: Cambridge (MA); 1972.

- [41] Peixinho J, Nouar C, Desaubry C, et al. Laminar transitional and turbulent flow of yield stress fluid in a pipe. J Non-Newtonian Fluid Mech. 2005;128:172–184. doi: 10.1016/j.jnnfm.2005.03.008
- [42] Blasius H. Das Ähnlichkeitsgesetz bei reibungsvorgängen in flussigkeiten. Forsch Arb Ing. 1913;134:1-41.
- [43] Browne LWB, Dinkelacker A. Turbulent pipe flow: pressures and velocities. J Fluid Dyn Res. 1995;15:177–204. doi: 10.1016/0169-5983(94)00038-2
- [44] Nikuradse J. Gesetzmssigkeiten der turbulenten strömung in glatten rohren. J Forschungsh Ver deutsch Ing. 1932;356:1–36.
- [45] Barenblatt GI. Scaling laws for fully-developed shear flows. Part 1. Basic hypotheses and analysis. J Fluid Mech. 1993;248:513–520. doi: 10.1017/S0022112093000874
- [46] Monkewitz PA, Nagib HM. The hunt for the kármán "constant" revisited. J Fluid Mech. 2023;967:A15. doi: 10.1017/jfm.2023.448
- [47] Millikan CM. A critical discussion of turbulent flows in channels and circular tubes. In: Proc. 5th Int. Congress of Appl. Mech. 1938. pp. 386–392.
- [48] Österlund JM, Johansson AV, Nagib HM, et al. A note on the overlap region in turbulent boundary layers. Phys Fluids. 2000;12:1–4. doi: 10.1063/1.870250
- [49] Wosnik M, Castillo L, George W. A theory for turbulent pipe and channel flows. J Fluid Mech. 2000;421:115–145 doi: 10.1017/S0022112000001385
- [50] von kármán T. Turbulence and skin friction. J Aero Sci. 1934;1:1-20. doi: 10.2514/8.5
- [51] Pashtrapanska M. ExperimentelleUntersuchung der turbulenten Rohrströmungen mit abklingender Drallkomponente [Ph.D. thesis]. Universität Erlangen Nürnberg. 2004.
- [52] Perry AE, Hafez S, Chong MS. A possible reinterpretation of the Princeton superpipe data. J Fluid Mech. 2001;439:395–401. doi: 10.1017/S0022112001004840
- [53] Smits AJ, Montey J, Multmark M, et al. Spatial resolution correction for wall–bounded turbulence measurements. J Fluid Mech. 2011;676:41–53. doi: 10.1017/jfm.2011.19
- [54] Hutchins N, Nickels TB, Marusic I, et al. Hot-wire spatial resolution issues in wall-bounded turbulence. J Fluid Mech. 2009;635:103–136. doi: 10.1017/S0022112009007721
- [55] Mathis R, Hutchins N, Marusic I. Large-scale amplitude modulation of the small-scale structures in turbulent boundary layers. J Fluid Mech. 2009;628:311–337. doi: 10.1017/S0022112009006946
- [56] Zanoun E-S, Egbers C, Örlü R, et al. Experimental evaluation of the mean momentum and kinetic energy balance equations in turbulent pipe flows at high Reynolds number. J Turbulence. 2019;20:1–15. doi: 10.1080/14685248.2019.1628968
- [57] Zanoun E-S, Durst F. Momentum transport and turbulent kinetic energy production in plane-channel flow. Int J Heat Mass Transf. 2009;52:4117–4124. doi: 10.1016/j.ijheatmasstransfer.2009.03.046
- [58] Hultmark M. A theory for the streamwise turbulent fluctuations in high Reynolds number pipe flow. J Fluid Mech. 2012;707:575–584. doi: 10.1017/jfm.2012.307
- [59] Hultmark1 M, Vallikivi1 M, Bailey SCC, et al. Logarithmic scaling of turbulence in smooth- and rough-wall pipe flow. J Fluid Mech. 2013;728:376–395. doi: 10.1017/jfm.2013.255
- [60] Nagib H, Vinuesa R, Hoyas S. Utilizing indicator functions with computational data to confirm nature of overlap in normal turbulent stresses:logarithmic or quarter-powe. Phys Fluids. 2024;36:075145. doi: 10.1063/5.0219031
- [61] Talamelli A, Segalini A, Örlü R, et al. A method to correct third and fourth order moments in turbulent flows. J Phys Conf Ser. 2011;318:042023. doi: 10.1088/1742-6596/318/4/042023
- [62] Bradshaw P. Inactive' motion and pressure fluctuations in turbulent boundary layers. J Fluid Mech. 1967;30:241–258. doi: 10.1017/S0022112067001417
- [63] McKeon BJ, Swanson CJ, Zagarola MV, et al. Friction factors for smooth pipe flow. J Fluid Mech. 2004;511:41–44. doi: 10.1017/S0022112004009796
- [64] Buschmann H, Gad-el-Hak M. Comment onevaluating the law of the wall in two-dimensional fully developed turbulent channel flows. Phys Fluids. 2003;15:3079–3089. Phys Fluids 2004 Sep;16(9):3507–3508. doi: 10.1063/1.1608010
- [65] Zanoun E-S, Durst F, Nagib H. Response tocomment onevaluating the law of the wall in two-dimensional fully developed turbulent channel flows. Phys Fluids. 2004;16:3507–3510. Phys Fluids. 2004 Sep;16(9):3509–3510. doi: 10.1063/1.1778789

Appendix. Estimation of the filtering effect due to insufficient resolution of the HWA probe

Here, we estimate the error induced by insufficient resolution of the HWA probe for the computation of streamwise velocity skewness and flatness profiles near the wall. Therefore, we applied a sharp spectral cutoff filter in the azimuthal direction to the velocity fields obtained from the DNS at $Re_{\tau}=2880$. The filter length was kept constant for all wall distances and corresponded to the length of the hot wire, i.e. $\lambda^+=48.2$ in wall units for $Re_{\tau}=2880$. Subsequently, the velocity statistics were computed by averaging in the axial and azimuthal directions, as well as over seven DNS snapshots. Figure A1 shows the streamwise velocity variance (a), the streamwise skewness (b), and the streamwise flatness (c) obtained from unfiltered DNS velocity fields (blue solid line), filtered DNS velocity fields (orange dashed line) and HWA measurements (green symbols).

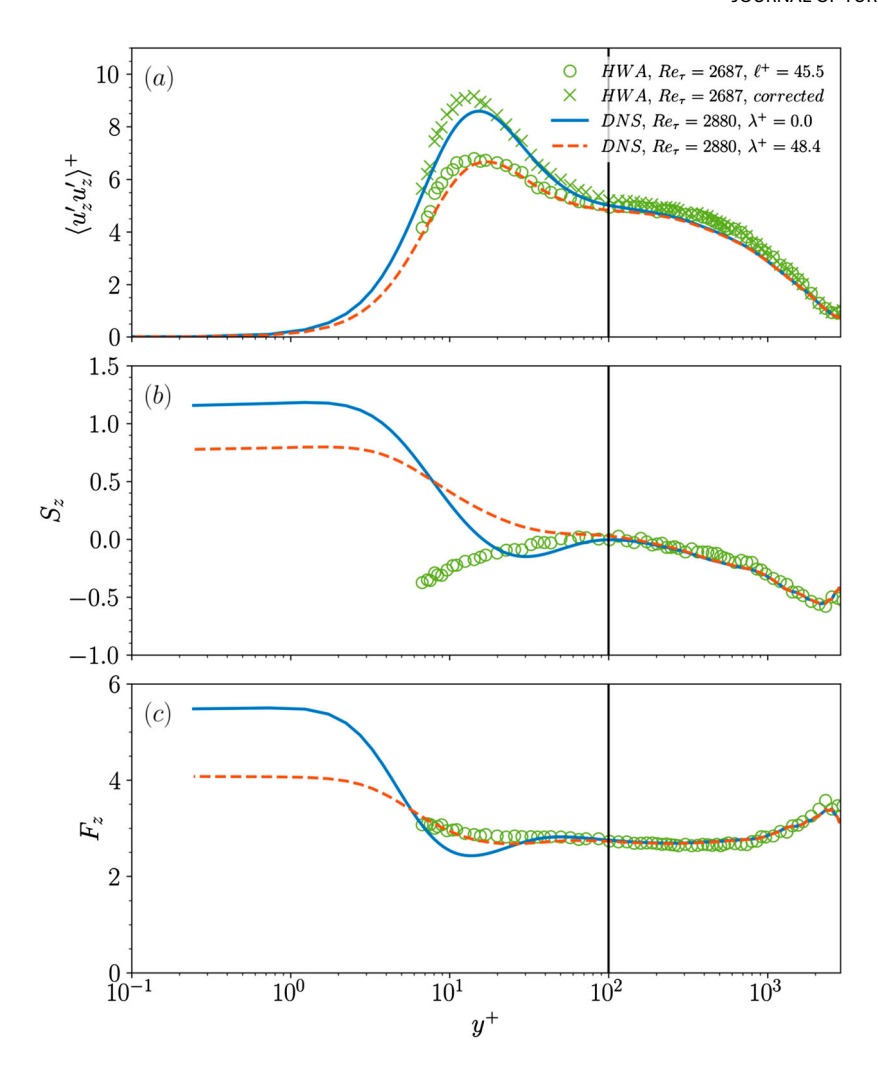


Figure A1. Streamwise velocity variance $\langle u_z' u_z' \rangle^+$ (a), skewness (b), and flatness (c), obtained from unfiltered DNS data at Re_{τ} = 2880 (blue solid line), filtered DNS data at Re_{τ} = 2880 (orange dashed line), and HWA measurements at Re_{τ} = 2687 (green symbols).

The filtered and unfiltered DNS profiles collapse for $y^+ \gtrsim 200$, while the filtering effect is clearly visible near the wall in all three statistical quantities. In addition, for the streamwise velocity skewness (Figure A1(b)), the HWA data collapse reasonably well with the unfiltered DNS data for $y^+ \gtrsim 80$.

In the following, the error induced by the filtering operation is estimated by subtracting the statistical profile of the filtered velocity $\hat{\phi}$ from the corresponding profile of the unfiltered velocity ϕ , see Figure A2. Note that error is normalised by the maximum of the statistical profile of the unfiltered velocity, because using a relative error would induce a singularity due to the zero crossing in the skewness profile. For the streamwise skewness (red dashed line in Figure A2), the error induced by filtering at the lower end of the reported collapse of the skewness profiles in Equation (12), i.e. $y^+ = 100$ is approximately two percent of the skewness maximum. Therefore, the reported collapse of the high Reynolds number DNS skewness profiles (Re $_{\tau} \geq 1500$) and the experimentally-measured skewness profiles at $100 \leq y^+ \leq 0.15 \text{Re}_{\tau} - \text{cf}$. Equation (12) – is assumed not to be significantly influenced by an artificial filtering effect due to the spatial resolution of the hot wire. Furthermore, the difference between the filtered and unfiltered streamwise velocity flatness profiles is less than two percent of the flatness maximum for $y^+ \geq 20$ (green dashed-dotted line in Figure A2), and the HWA data collapses well with the unfiltered DNS profile for $y^+ \gtrsim 40$ (cf. Figure A1(c)). Consequently, the effect of insufficient resolution of the HWA probe is assumed to be minor only at the near-wall end of the suggested scaling of the streamwise velocity flatness for $50 \leq y^+ \leq 300$ in Equation (14).

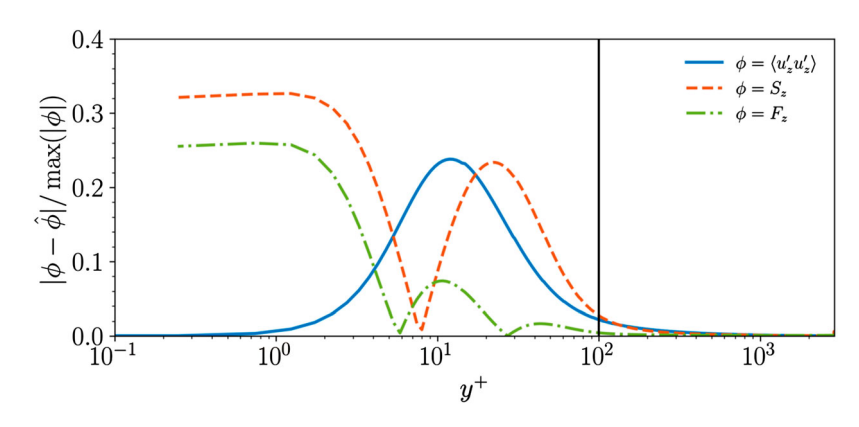


Figure A2. Error of the streamwise velocity variance $\langle u_z'u_z'\rangle^+$ (blue solid line), skewness S_z (red dashed line), and flatness F_z (green dashed-dotted line) due to filtering of the velocity field with a spanwise filter length of $\lambda^+=48.2$ in wall units. DNS data, $Re_{\tau} = 2880$.